

©2018. American Geophysical Union. All Rights Reserved

Access to this work was provided by the University of Maryland, Baltimore County (UMBC) ScholarWorks@UMBC digital repository on the Maryland Shared Open Access (MD-SOAR) platform.

**Please provide feedback**

Please support the ScholarWorks@UMBC repository by emailing [scholarworks-group@umbc.edu](mailto:scholarworks-group@umbc.edu) and telling us what having access to this work means to you and why it's important to you. Thank you.

## RESEARCH ARTICLE

10.1002/2014JC009803

## Key Points:

- Urban coastal regions are characterized by strong variability in atmospheric NO<sub>2</sub>
- If not adequately corrected, NO<sub>2</sub> can have a major impact on coastal OC retrievals
- Unaccounted NO<sub>2</sub> results in false diurnal changes in coastal Rrs, Chla, and CDOM

## Correspondence to:

M. Tzortziou,  
martz@umd.edu

## Citation:

Tzortziou, M., J. R. Herman, Z. Ahmad, C. P. Loughner, N. Abuhassan, and A. Cede (2014), Atmospheric NO<sub>2</sub> dynamics and impact on ocean color retrievals in urban nearshore regions, *J. Geophys. Res. Oceans*, 119, 3834–3854, doi:10.1002/2014JC009803.

Received 8 JAN 2014

Accepted 24 MAY 2014

Accepted article online 3 JUN 2014

Published online 19 JUN 2014

Atmospheric NO<sub>2</sub> dynamics and impact on ocean color retrievals in urban nearshore regions

Maria Tzortziou<sup>1</sup>, Jay R. Herman<sup>2,3</sup>, Ziauddin Ahmad<sup>3,4</sup>, Christopher P. Loughner<sup>1</sup>, Nader Abuhassan<sup>2,3</sup>, and Alexander Cede<sup>3,5</sup>
<sup>1</sup>Earth System Science Interdisciplinary Center, University of Maryland, College Park, Maryland, USA, <sup>2</sup>Joint Center for Earth Systems Technology, University of Maryland, Baltimore, Maryland, USA, <sup>3</sup>NASA Goddard Space Flight Center, Greenbelt, Maryland, USA, <sup>4</sup>Science and Data Systems, Inc., Silver Spring, Maryland, USA, <sup>5</sup>LuftBlick, Kreith, Austria

**Abstract** Urban nearshore regions are characterized by strong variability in atmospheric composition, associated with anthropogenic emissions and meteorological processes that influence the circulation and accumulation of atmospheric pollutants at the land-water interface. If not adequately corrected in satellite retrievals of ocean color, this atmospheric variability can impose a false impression of diurnal and seasonal changes in nearshore water quality and biogeochemical processes. Consideration of these errors is important for measurements from polar orbiting ocean color sensors but becomes critical for geostationary satellite missions having the capability for higher frequency and higher spatial resolution observations of coastal ocean dynamics. We examined variability in atmospheric NO<sub>2</sub> over urban nearshore environments in the Eastern US, Europe, and Korea, using a new network of ground-based Pandora spectrometers and Aura-OMI satellite observations. Our measurements in the US and in Europe revealed clear diurnal and day-of-the-week patterns in total column NO<sub>2</sub> (TCNO<sub>2</sub>), temporal changes as large as 0.8 DU within 4 h, and spatial variability as large as 0.7 DU within an area often covered by just a single OMI pixel. TCNO<sub>2</sub> gradients were considerably stronger over the coastal cities of Korea. With a coarse resolution and an overpass at around 13:30 local time, OMI cannot detect this strong variability in NO<sub>2</sub>, missing pollution peaks from industrial and rush hour activities. Observations were combined with air quality model simulations and radiative transfer calculations to estimate the impact of atmospheric NO<sub>2</sub> variability on satellite retrievals of coastal ocean remote sensing reflectance and biogeochemical variables (i.e., chlorophyll and CDOM).

## 1. Introduction

Among the major challenges in accurate retrievals of coastal ocean optical properties and biogeochemical processes from space is detecting the small contribution of water-leaving radiances to the total radiance at the top of the atmosphere (TOA). The ocean contribution to the total TOA signal measured in the blue part of the spectrum by a satellite ocean color (OC) sensor is typically <10% in open ocean waters, but can be <1% in optically complex coastal and estuarine environments with large concentrations of strongly absorbing particles and aromatic dissolved organic compounds [IOCCG, 2010]. To interpret the small signal from the ocean, an accurate atmospheric correction must be derived using radiative transfer models to subtract atmospheric Rayleigh scattering, aerosol attenuation, ozone absorption, and other atmospheric absorbers [Gordon and Voss, 1999].

An added complication for nearshore waters close to heavily polluted urban centers is the strong temporal variability and spatial gradients in atmospheric absorbing aerosols and trace gases, associated with anthropogenic activities from industrial emissions, motor vehicles, construction, and power generation. Sea-breeze and land-breeze circulations largely affect advection, recirculation, and accumulation of atmospheric pollutants at the land-water interface, leading to buildup of emissions and aggravation of air pollution along the shoreline [Kallos et al., 1993; Tie et al., 2009; Kanakidou et al., 2011; von Glasow et al., 2013]. Models have shown that strong, prolonged sea or bay-breeze events can transport a large amount of urban air pollution out of the planetary boundary layer and into the free troposphere where pollutants have longer lifetime and are susceptible to long-range transport offshore and over adjacent ocean environments [Loughner et al., 2014]. For improperly or partially corrected satellite observations, such variability in atmospheric composition can cause a false retrieval of variability in nearshore water optical and biogeochemical properties [Fishman et al., 2012].

The impact of aerosols on satellite retrievals of inland and coastal water bio-optical properties has been studied extensively during the last decades. Several correction algorithms have been proposed and incorporated into the processing of satellite ocean color imagery [e.g., *Gordon and Wang*, 1994; *Siegel et al.*, 2000; *Ruddick et al.*, 2000; *Stumpf et al.*, 2003; *IOCCG*, 2010; *Wang et al.*, 2012]. Retrievals of underwater properties are usually limited to scenes with low aerosol amounts by flagging/masking ocean color pixels under high aerosol optical thickness conditions [*Gordon and Wang*, 1994]. Still, this leaves uncorrected ocean color scenes affected by absorbing trace gases.

With an absorption signature that extends from the UV (270 nm) to the near-IR (~770 nm) and peaks near 410 nm [*Harder et al.*, 1997; *Vandaele*, 1998], nitrogen dioxide ( $\text{NO}_2$ ) is a key absorbing trace gas that affects the TOA signal measured by an OC satellite sensor at wavelengths traditionally used for chlorophyll-a (*Chla*) and colored dissolved organic matter (CDOM) retrievals [e.g., *O'Reilly et al.*, 2000; *Carder et al.*, 2003; *Mannino et al.*, 2008; *Le and Hu*, 2013]. Biomass burning, lightning, aviation, soil microbial production, fossil fuel combustion from motor vehicles, industrial activities, and currently unregulated ship emissions are major sources of nitrogen oxides ( $\text{NO}_x$ ) in nearshore regions [e.g., *Lee et al.*, 1997; *Davis et al.*, 2001; *Endresen et al.*, 2003; *Richter et al.*, 2004; *Franke et al.*, 2009].  $\text{NO}_x$  pollution and its partial conversion to  $\text{NO}_2$  remains a serious problem in many coastal cities worldwide, both in industrialized and, particularly, in developing economies where rapid coastal urbanization is presently occurring [e.g., *Martinelli et al.*, 2006; *Pineda Rojas and Venegas*, 2009; *Gu et al.*, 2011]. Yet the impact of atmospheric  $\text{NO}_2$  absorption on retrievals of inland, estuarine, and coastal water remote sensing reflectance and biogeochemical variables has been, until recently, largely ignored [*Ahmad et al.*, 2007; *Herman et al.*, 2009; *Tzortziou et al.*, 2013].

Measurements of  $\text{NO}_2$  from both ground and space-based instruments have highlighted the importance of urban areas as hot spots of  $\text{NO}_x$  emissions and the influence of various  $\text{NO}_x$  sources on local and trans-boundary pollution episodes [*Wenig et al.*, 2003; *Beirle et al.*, 2004; *Boersma et al.*, 2005; *Choi et al.*, 2005]. Satellite measurements with GOME-1 (Global Ozone Monitoring Experiment) [*Burrows et al.*, 1999], SCIAMACHY (SCanning Imaging Absorption spectroMeter for Atmospheric CHartography) [*Bovensmann et al.*, 1999], GOME-2 [*Callies et al.*, 2000], and OMI (Ozone Monitoring Instrument) [e.g., *Levelt et al.*, 2006; *Celarier et al.*, 2008] have provided valuable information on the spatial variability of  $\text{NO}_2$  and its seasonal patterns. Comparisons of measurements from different satellite instruments have revealed large differences between morning and afternoon total column  $\text{NO}_2$  ( $\text{TCNO}_2$ ) amounts, driven by emissions and photochemistry [e.g., *Richter et al.*, 2005; *Boersma et al.*, 2008]. Much higher frequency measurements from networks of ground-based instruments, such as the Pandora spectrometer systems (approximately once per minute) [*Herman et al.*, 2009], have provided the capability to capture the strong temporal and spatial variability typically characterizing atmospheric composition in polluted urban areas [*Tzortziou et al.*, 2012, 2013; *Reed et al.*, 2013]. Frequently,  $\text{TCNO}_2$  changes exceed 0.5 DU over a period of an hour, and 1 DU over a period of less than 3 h [*Herman and Tzortziou*, 2011; *Herman et al.*, 2009].

Transport of air masses with such variable  $\text{NO}_2$  amounts over coastal areas will have a large influence on satellite estimates of coastal ocean remote sensing reflectance in the UV-green spectral region (350–550 nm), affecting retrievals of other ocean color products. Previous radiative transfer calculations [*Ahmad et al.*, 2007] showed that a change in  $\text{NO}_2$  by 0.37 DU ( $=10^{16}$  molecules/ $\text{cm}^2$ ) decreases the TOA reflectance in the blue channels of OC sensors such as SeaWiFS (Sea-viewing Wide Field-of-view Sensor) and MODIS (Moderate-resolution Imaging Spectroradiometer) by approximately 0.6–0.9%, depending, among other factors, on the  $\text{NO}_2$  vertical distribution. A change of this magnitude in the TOA reflectance in the blue spectral region translates into approximately a 10% error in ocean remote sensing reflectance,  $R_{rs}$ , for clear waters and larger errors (>20%) in coastal areas [*Ahmad et al.*, 2007]. *Ahmad et al.* [2007] showed that incorporation of an  $\text{NO}_2$  atmospheric correction in the processing of almost aerosol-clear (low AOT) MODIS ocean color imagery over the Eastern US coast resulted in higher nLw values over high  $\text{NO}_2$  concentration areas and in a significant decrease in the frequency of negative nLw estimates.

Based on this initial work, partial  $\text{NO}_2$  corrections were added in the most recent reprocessing of NASA satellite ocean color data, using a monthly  $\text{NO}_2$  climatology derived from GOME, SCIAMACHY, and OMI [*Robinson et al.*, 2007]. However, among the main issues of using these satellite data for atmospheric correction of ocean color is their much coarser spatial resolution relative to satellite ocean color observations (i.e., 12 km  $\times$  24 km at nadir view for OMI, and even coarser for GOME and SCIAMACHY, relative to 1 km  $\times$  1 km at nadir for MODIS). Use of monthly climatology does not account for the high  $\text{NO}_2$  temporal (weekly, diurnal,

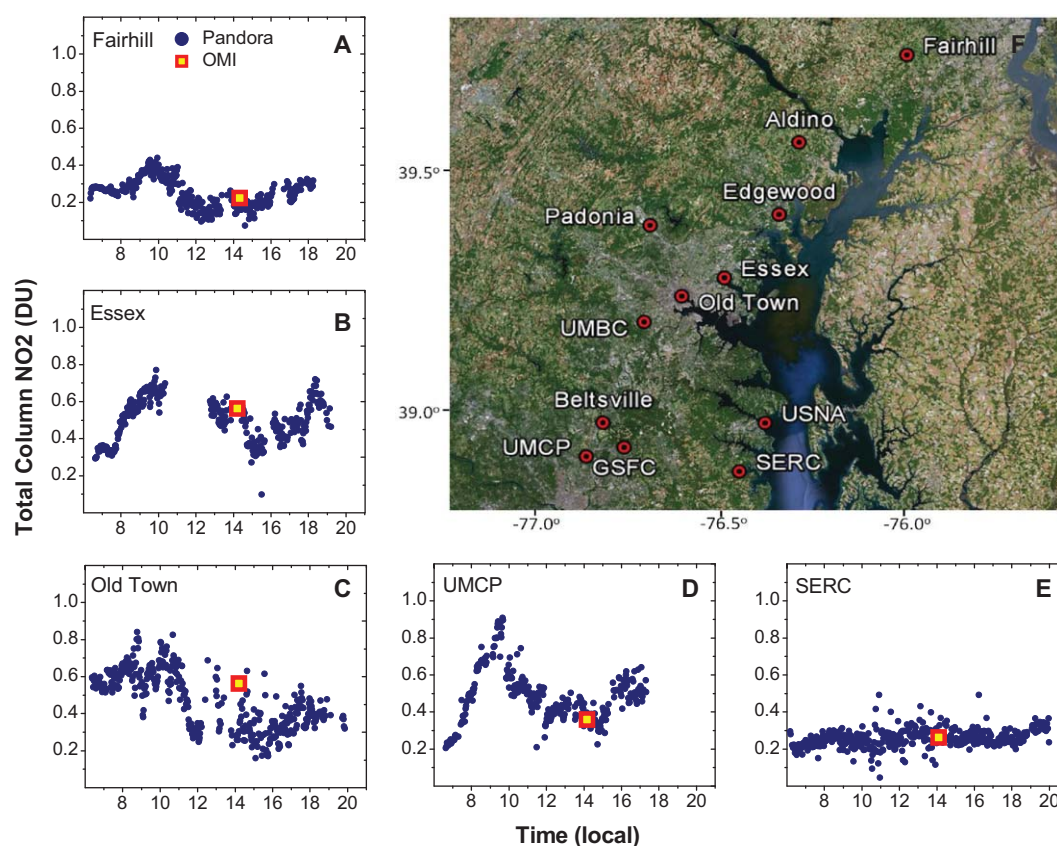


**Figure 1.** Total column NO<sub>2</sub> amounts measured by Pandora (circles) and Aura-OMI (squares) at five sites in the Washington/Baltimore urban area and along the Chesapeake shore: (a) Fairhill, (b) Essex, (c) Old Town (d) UMCP and (e) SERC, during a typical, relatively low pollution summer weekday on 18 July 2011. A map with the location of all Pandora sites in this region is provided in Figure 1f.

and hourly) variability reported for urban coastal areas [Tzortziou *et al.*, 2013], or even properly account for seasonal affects [Cede *et al.*, 2006]. Even daily OMI images fail to capture weekly and diurnal patterns and peaks in NO<sub>2</sub> associated with human activities in coastal urban areas [Tzortziou *et al.*, 2013]. Consideration of these error sources is important for measurements from the current generation of polar orbiting OC satellite sensors, but becomes critical for recently launched and future geostationary satellite missions that aim at providing higher frequency observations of ocean dynamics and diurnal variability.

Global constellations of geostationary atmospheric chemistry and coastal ocean color sensors are a possibility by 2020 [Fishman *et al.*, 2012]. The Korea Aerospace Research Institute (KARI) recently launched the Geostationary Ocean Color Imager (GOCI) with follow-on plans for a GOCI-II launch in 2018. The Geostationary for Coastal and Air Pollution Events (GEO-CAPE) mission is one of NASA's Decadal Survey missions recommended for launch by the U.S. National Research Council (NRC) [Fishman *et al.*, 2012]. There is interest by European and Indian space agencies to launch geostationary OC sensors in the 2020 time frame as well [IOCCG, 2012]. The requirement for high spatial and temporal resolution observations associated with the science objectives of these missions (e.g., 250–500 m at nadir, and 1 h refresh rate for GOCI and GOCI-II) provides a unique capability for detecting, monitoring, and eventually improving prediction of small scale and short-term coastal ocean processes and dynamics. However, temporally resolved ocean color observations may require nearly coincident satellite retrievals of absorbing atmospheric constituents, such as NO<sub>2</sub>, to avoid aliasing atmospheric absorption variability for changes in ocean composition.

Here we present new measurements of coastal NO<sub>2</sub> variability from Pandora and Aura-OMI along the Chesapeake Bay estuarine shoreline in the Eastern US, in Helsinki on the shore of the Gulf of Finland in the Baltic Sea, and in the Korean coastal megacities of Seoul and Busan along the Yellow and East Seas. These measurements illustrate the strong NO<sub>2</sub> temporal and spatial gradients typically observed in moderately to highly polluted coastal urban areas in both developed and developing countries. We estimate the impact of

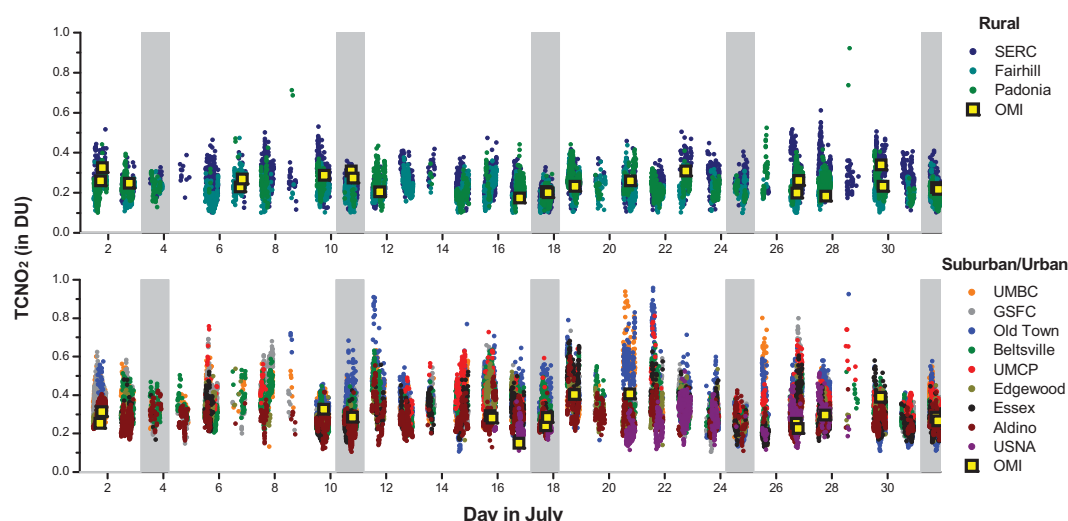


**Figure 2.** Spatial and temporal variability in  $\text{TCNO}_2$  (in DU) as observed by the Pandora network over the Washington DC/Chesapeake Bay area during the Discover-AQ campaign. Different Pandora sites are shown with different color (solid circles) and are grouped from (top) rural to (bottom) suburban-urban. OMI overpass  $\text{TCNO}_2$  retrievals are also shown (squares). Measurements on Sundays are indicated by the shaded area.

$\text{NO}_2$  absorption on the TOA signal and subsequent errors in ocean  $R_{rs}$  caused by not accounting appropriately for  $\text{NO}_2$  variability during ocean color atmospheric correction. We focus on the problems associated with geostationary measurements, since the main purpose of geostationary satellite ocean color observations is resolving and understanding temporal variability in ocean processes. The implications of using currently available satellite  $\text{NO}_2$  data (e.g., OMI) in atmospheric correction retrievals for polar orbiting OC sensors are also discussed. Errors in satellite-retrieved in-water biogeochemical variables, resulting from errors in  $R_{rs}$ , are calculated based on OC algorithms used for standard *Chla* products and peer-reviewed published retrievals for CDOM.

## 2. Methods

### 2.1. Study Sites

#### 2.1.1. Chesapeake Bay Estuarine Environment

To characterize spatial and temporal variability of total column  $\text{NO}_2$  amounts near urban pollution sources and estuarine environments, we deployed a network of Pandora spectrometers systems at key locations within the broader Washington/Baltimore urban area and along the western shoreline of the Chesapeake Bay (Figure 1f) [Tzortziou *et al.*, 2013]. Emissions associated with transportation, natural sources (e.g., soils), and transport of background pollution from upwind locations all play an important role in causing poor air quality over this region. Meteorological processes along the Chesapeake Bay land-sea interface and meso-scale phenomena, such as bay-breeze circulations, additionally impact transport and transformation of atmospheric pollutants both over land and over the estuary [Loughner *et al.*, 2011, 2014]. The sites of the Pandora network are characterized by varying levels of pollution and anthropogenic influences, ranging from rural (SERC-Smithsonian Environmental Research Center, Fairhill, and Padonia sites), to suburban (Edgewood, Essex, Aldino, and USNA-US Naval Academy), to urban (UMBC-University of Maryland Baltimore County, GSFC-Goddard Space flight Center, Old Town in Baltimore, Beltsville, and UMCP-University of Maryland College Park) (Figure 2). Among these sites, the longest time series is available for GSFC, a moderately polluted site in Greenbelt, MD, with long-term and ongoing monitoring of atmospheric composition from various instruments including CIMEL sun-photometers, a modified Mark III Brewer double monochromator (#171), Pandora instruments, and shadow-band spectrometers [Holben *et al.*, 1998; Krotkov *et al.*, 2005; Cede *et al.*, 2006; Herman *et al.*, 2009; Tzortziou *et al.*, 2012, 2013]. Measurements of total column  $\text{NO}_2$  have been performed on the roof of a building (88 m a.s.l.) at GSFC since 2006 using both Brewer (#171) and Pandora instruments. The site is located close to two major highway systems that are strong sources of  $\text{NO}_x$ .



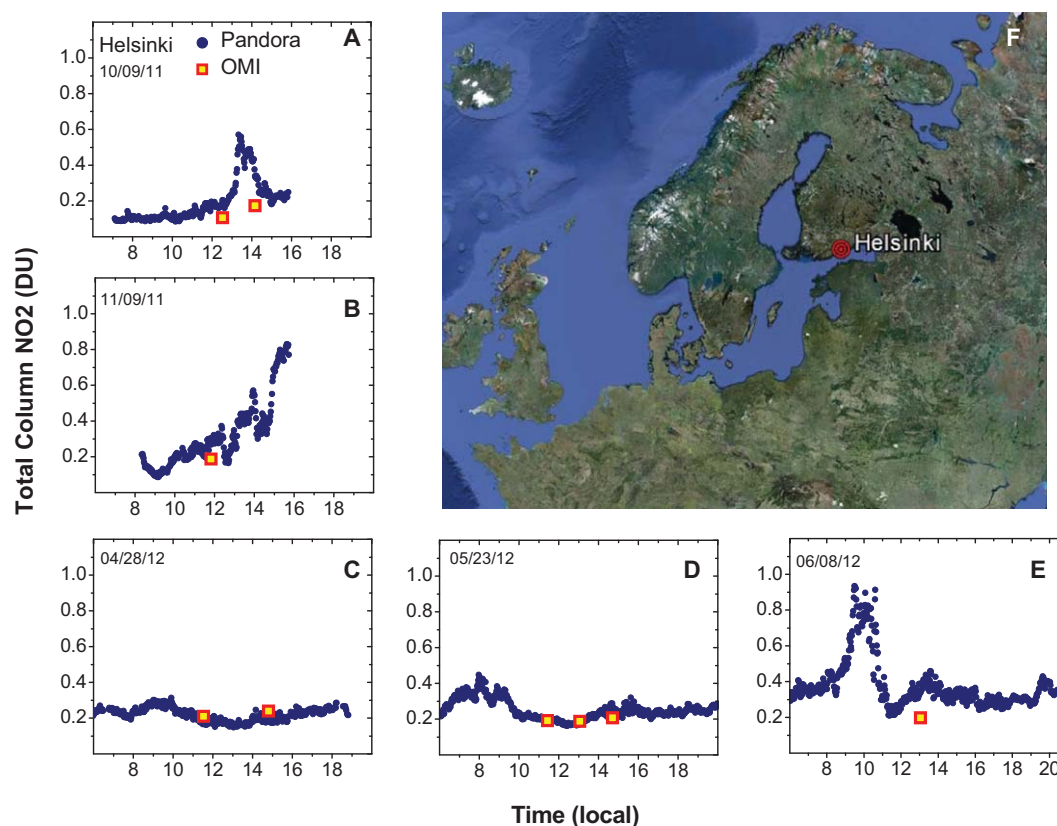


**Figure 3.** Diurnal variability in total column  $\text{NO}_2$  amounts measured by Pandora (#21) (circles) and Aura-OMI (squares) in Helsinki, Finland on (a) 9 October 2011, (b) 9 November 2011, (c) 28 April 2012, (d) 23 May 2012, and (e) 8 June 2012. A map with the location of the Pandora site is provided in Figure 3f.

emissions resulting in strong spatial inhomogeneity and rapid changes in local tropospheric composition [Herman *et al.*, 2009; Tzortziou *et al.*, 2012].

Detailed Pandora measurements were performed at strategic locations within the Chesapeake Bay urban air-shed during July–August 2011, as part of two simultaneous NASA field campaigns in the region: the DISCOVER-AQ (Deriving Information on Surface Conditions from Column and Vertically Resolved Observations Relevant to Air Quality) and the GeoCAPE-CBODAQ (Geostationary Coastal and Air Pollution Events–Chesapeake Bay Oceanographic Campaign with DISCOVER-AQ) field campaigns [Tzortziou *et al.*, 2013]. Among the major objectives of these campaigns was to collect detailed field (ground-based, shipboard, and airborne) observations to improve interpretation of satellite atmospheric and ocean color observations and enhance remote sensing retrievals of coastal air quality and ocean biogeochemical processes [Crawford and Pickering, 2011; Tzortziou *et al.*, 2013]. An intercomparison campaign for 11 Pandoras was performed at the GSFC site at the end of the DISCOVER-AQ and CBODAQ campaigns, to determine instrument performance characteristics under the same conditions and detect any consistent instrument offsets. Detailed results from the intercomparison are provided in Tzortziou *et al.* [2013]. Briefly, intercalibration results showed excellent agreement among the different Pandora spectrometers after the campaigns were completed. Absolute average differences in  $\text{TCNO}_2$  had almost zero air-mass-factor dependence and were in all cases less than 0.07 DU, with most Pandoras showing average differences less than 0.02 DU (or 5%). These results suggest that the spatial variability in  $\text{NO}_2$  measured by the different Pandora instruments in the Baltimore/Washington area and Chesapeake Bay estuary during the 2011 campaign was real and not due to instrument offsets [Tzortziou *et al.*, 2013].

### 2.1.2. Helsinki, Finland

In September 2011, Pandora system #21 was deployed in Helsinki, Finland (Lat = 60.204°N, Long = 24.961°E) (Figure 3f) and has been taking measurements at this coastal location since then as part of a

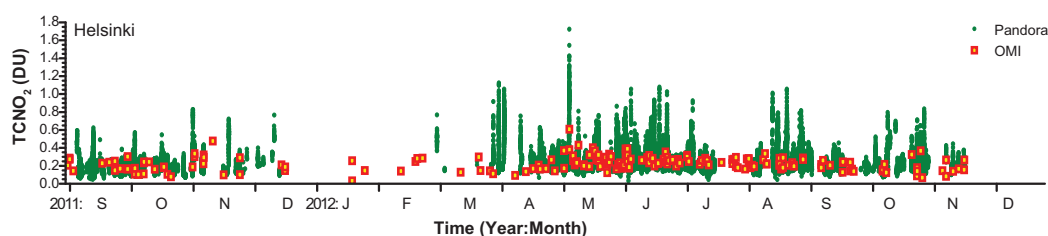


**Figure 4.** NO<sub>2</sub> variability over Helsinki from September 2011 (when Pandora #21 was deployed at FMI) to November 2012. OMI overpass TCNO<sub>2</sub> retrievals are also shown (squares).

larger effort focusing on measurements of atmospheric trace gas (NO<sub>2</sub>, O<sub>3</sub>, HCHO, and BrO) dynamics in high-latitude environments. The instrument is located on top of the Finnish Meteorological Institute (FMI), in an area of moderate automobile traffic with frequently maritime and occasionally polluted air masses. Instrument performance and retrievals of total column ozone (TCO<sub>3</sub>) have been previously discussed for this site, and other mid to high-latitude sites in Europe and in the US, in Tzortziou *et al.* [2012]. Pandora and Aura-OMI TCO<sub>3</sub> retrievals were found to be in very good agreement, with average residuals of <1%, when the OMI cross track position was at a distance of less than 50 km from the Pandora location and OMI-measured cloud fraction was less than 0.2. Tzortziou *et al.* [2012] reported relatively low total column ozone diurnal variation in Helsinki, compared to other mid to high-latitude sites, with observed amplitude in TCO<sub>3</sub> diurnal variation having an average value of 12 DU (or, 4–5%) and a maximum of 33 DU.

### 2.1.3. Korean Coastal Megacities

To examine trace gas variability in coastal urban areas in developing countries that suffer by increasing anthropogenic pollution, two Pandora spectrometers were deployed in Seoul and Busan in South Korea in March 2012 (Figure 5f). Data discussed in this paper cover the period from March 2012 to March 2013 (Figure 6). Seoul (37.017°N, 126.967°E) is the capital and largest metropolis of South Korea, a megacity with a population of over 10 million. The city is located almost 20 km inland from the Yellow (or East China) Sea. The coastal city of Busan (35.083°N, 129.000°E) is South Korea's largest port and second largest metropolis after Seoul, with a population of around 3.6 million. Busan is located on the southeastern-most tip of the Korean peninsula, along the coast of the East Sea (Figure 5f). Both cities are characterized by high levels of air pollution and NO<sub>x</sub> emissions, associated with increased urbanization and industrialization, as well as trans-boundary pollution from other highly polluted urban centers in East Asia, including Tokyo, Shanghai, and Beijing [e.g., Pandey *et al.*, 2008; Guttikunda *et al.*, 2005].

## 2.2. Measurements of Total Column NO<sub>2</sub>

### 2.2.1. Pandora Retrievals

A detailed description of the Pandora instrument technical characteristics is provided in Herman *et al.* [2009] and in Tzortziou *et al.* [2012, 2013]. Briefly, the Pandora spectrometer system (280–525 nm) consists of an optical head sensor, mounted on a computer controlled sun-tracker and sky-scanner (~0.01° pointing precision) and connected to an Avantes array spectrometer by means of a 400 micron core-diameter single strand multimode optical fiber. To achieve wavelength and radiometric calibration stability, the spectrometer is temperature stabilized inside an insulated enclosure using an actively coupled thermo-electric cooler and heater. Pandora has a spectral resolution of 0.6 nm and a field of view (FOV) of about 1.6° full width half maximum (FWHM). Wavelength calibration and slit functions are determined from lamp emission lines (Hg, Cd, Cu, In, Mg, and Zn). Wavelength stability is validated during field use by an analysis of the solar Fraunhofer line structures. Here we analyze TCNO<sub>2</sub> amounts derived from Pandora spectrometers operated in direct-sun viewing mode. The spectral fitting algorithm uses laboratory measured absorption cross sections for each atmospheric absorber, a fourth-order polynomial in wavelength to remove aerosols and Rayleigh scattering effects, and wavelength shift and squeeze functions to remove wavelength errors at the 1 picometer level. The shift and squeeze functions provide the best match to the measured spectrum compared to a solar reference spectrum containing the solar Fraunhofer line structure [Herman *et al.*, 2009; Tzortziou *et al.*, 2013].

Pandora's direct-sun TCNO<sub>2</sub> includes both the troposphere and the stratosphere, with a stratospheric contribution of typically 0.1–0.2 DU. The TCNO<sub>2</sub> retrieval uses laboratory NO<sub>2</sub> absorption cross sections [Vandaele

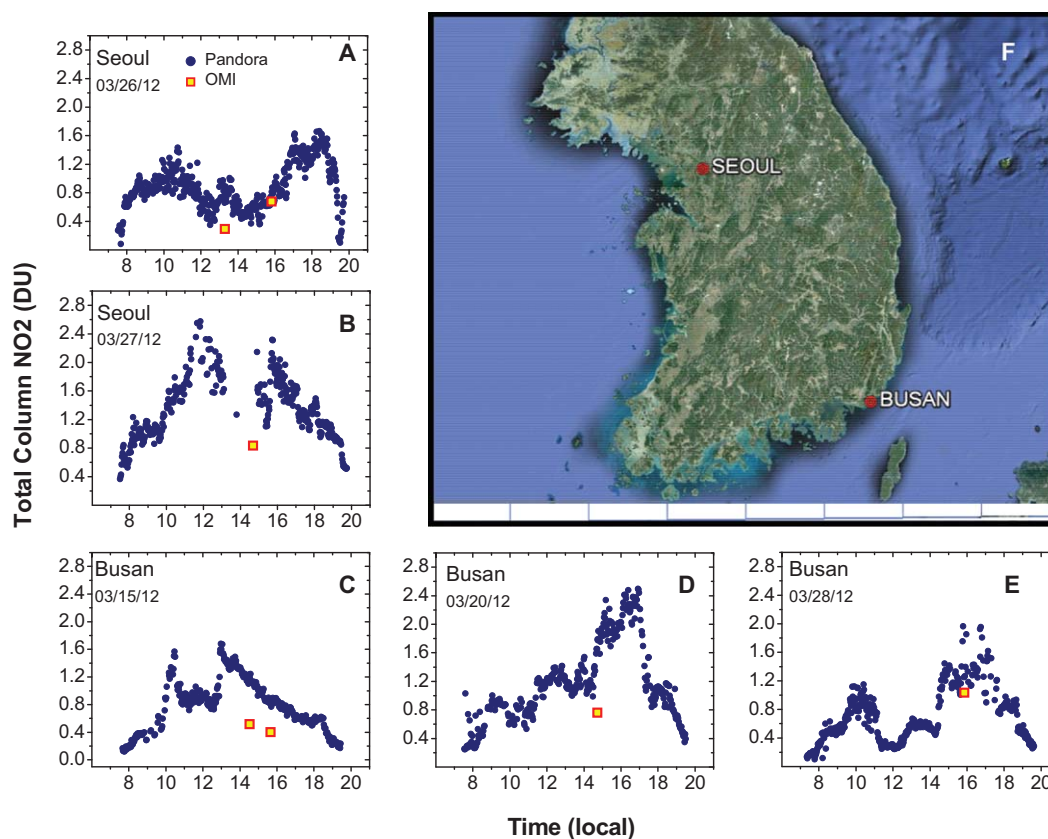


**Figure 5.** Diurnal variability in total column NO<sub>2</sub> amounts measured by Pandora (circles) and Aura-OMI (squares) in South Korea. (a) Seoul, 3/26/12, (b) Seoul, 3/27/12, (c) Busan, 3/15/12, (d) Busan, 3/20/12, (e) Busan, 3/28/12. A map with the location of the Pandora sites in South Korea is provided in Figure 5f.

*et al.*, 1998] and laboratory calibration of Pandora (wavelength, slit function, and radiometric). The retrieval is done by spectral fitting over the range 400–440 nm. Absolute error in Pandora TCNO<sub>2</sub> retrievals is 0.1 DU, caused by an error in estimating residual stratospheric NO<sub>2</sub> amount by extrapolating to zero air mass using a modified Langley method [Herman *et al.*, 2009]. The modern CCD version of the Pandora has a precision of about 0.01 DU in clear skies from averaging about 4000 measurements in a 20 s interval, where the exposure time is adjusted to fill the CCD wells to about 80%. In the presence of clouds the exposure time increases so that fewer measurements are averaged per 20 s, which reduces the precision.

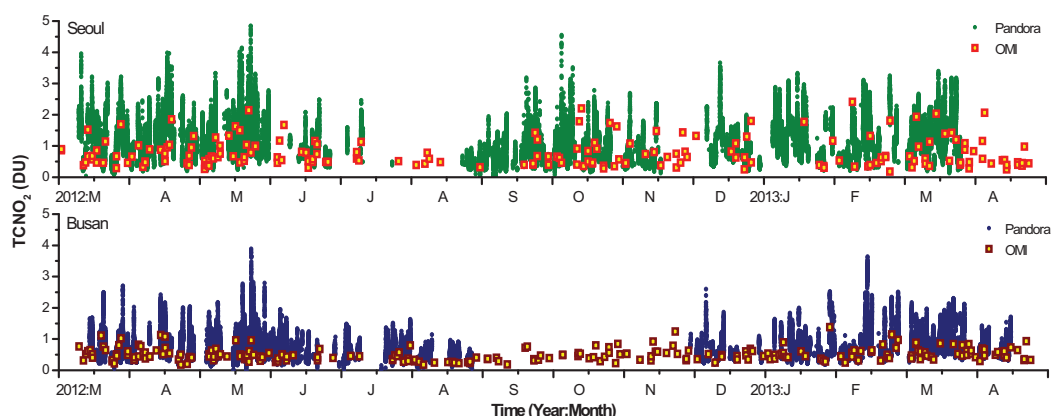


**Figure 6.** NO<sub>2</sub> variability over (top) Seoul and (bottom) Busan since March 2012 when Pandora spectrometers were deployed at these locations. OMI overpass TCNO<sub>2</sub> retrievals are also shown (squares).



### 2.2.2. OMI Retrievals

The Ozone Monitoring Instrument (OMI), launched on NASA's Earth Observing System (EOS) AURA satellite on 15 July 2004, has been collecting data since 9 August 2004 [Levelt et al., 2006; Boersma et al., 2007]. AURA has a sun-synchronous polar orbit at approximately 705 km altitude with a period of 100 min and a local equator crossing time between 13:40 and 13:50 local time. OMI is a cross-track downward viewing near-UV/Visible CCD spectrometer that provides near-global coverage in 1 day. The size of an OMI pixel varies with cross-track viewing zenith angle from 24 km in the nadir to approximately 128 km for the extreme viewing angles of 57° at the edges of the swath [Boersma et al., 2007]. OMI measurements cover a spectral region of 264–504 nm with a spectral resolution between 0.42 nm and 0.63 nm and provide retrievals of a number of trace gases including O<sub>3</sub>, NO<sub>2</sub>, SO<sub>2</sub>, HCHO, BrO, and OCIO.

The EOS Aura OMI OMNO2-L2OVP (Data Set Version 003) NO<sub>2</sub> product is used in this study (<http://avdc.gsfc.nasa.gov>, data set release date: July 2012). This product contains the slant column NO<sub>2</sub> (total amount along the optical path from the sun into the atmosphere, reflected by Rayleigh scattering and the earth's surface back toward the satellite), the total vertical column NO<sub>2</sub>, and the estimated tropospheric portion of the total column NO<sub>2</sub>. Uncertainties in magnitude of the air mass factor, NO<sub>2</sub> profile shape, and surface reflectivity are major sources of error. Other ancillary data are also provided in the OMI OMNO2-L2OVP file, including data quality flags, measures of precision, and quality assurance information. The slant column amount NO<sub>2</sub> is determined from a spectral fit to the Earth reflectance spectrum using the Differential Optical Absorption Spectroscopy (DOAS) method [Platt, 1994; Boersma et al., 2002; Bucsela et al., 2006]. The fitting algorithm is applied in the spectral range 405–465 nm using the Vandaele et al. [1998] NO<sub>2</sub> absorption cross sections convoluted with the measured OMI slit function. Total vertical column NO<sub>2</sub> amounts are estimated from the measured slant column using computed air mass factors (AMFs) and a monthly mean climatology of NO<sub>2</sub> profile shapes constructed from the Global Modeling Initiative (GMI) Chemical Transport Model simulation [Palmer et al., 2001; Krotkov and OMI NO<sub>2</sub> Algorithm Team, 2012].

Pandora results are compared here with OMI TCNO<sub>2</sub> station overpass data (<http://avdc.gsfc.nasa.gov/index.php?site=1593048672&id=28>). OMI station overpass data files provide the nearest OMI measurement in an OMI track (orbit), if it is closer than 100 km, to the ground station. Among other parameters, the data files contain information on the distance between the overpass location point and the OMI FOV, the OMI cross track position CTP (0–59), and the radiative cloud fraction.

### 2.3. Radiative Transfer Calculations

Radiative transfer simulations were performed using two radiative transfer programs originally developed, respectively, by Ahmad and Fraser [1982] and Mobley [1988, 1994]. We have linked the two codes, so that output from one code is provided as input to the other for a more complete and accurate description of the ocean-atmosphere system.

The Hydrolight underwater radiative transfer numerical model [Mobley, 1988] was used to estimate water-leaving radiances,  $L_w(\lambda)$ , and remote sensing reflectance spectra,  $R_{rs}(\lambda)$ , following the approach in Tzortziou et al. [2006]. Model runs were performed for water properties typical of optically complex nearshore waters, based on bio-optical measurements performed in the Chesapeake Bay estuarine waters during September 2001 [Tzortziou et al., 2007]. More specifically, Hydrolight calculations were performed for average *Chla* concentration of 23 mg m<sup>-3</sup>, total suspended solids concentration of 20 mg m<sup>-3</sup>, and average CDOM absorption of 2.1 m<sup>-1</sup> at 300 nm.

The Ahmad-Fraser (AF) code was used to compute the upwelling and downwelling radiances at the top and bottom of the atmosphere using the vector formulation (Stokes parameters) of the radiative transfer equation. The AF code can simulate radiances from ultraviolet (~300 nm) to short-wave IR (~3.0 μm) for any realistic model of atmosphere consisting of standard gas (air), aerosols (both absorbing and nonabsorbing), and trace gases (e.g., ozone and NO<sub>2</sub>). These simulations were performed using a flat ocean surface. Among other quantities, the Hydrolight code provided estimates of  $R_{rs}(\lambda)$  just above the ocean surface. The AF code has the capability to accept any spectrum of  $R_{rs}(\lambda)$  and compute the TOA reflectance,  $\rho_{TOA}(\lambda)$ , for any atmospheric condition over a flat or a rough ocean. We used this capability to simulate the TOA reflectance for variable NO<sub>2</sub> total column amounts and vertical distribution. In these simulations,  $L_w$  was assumed to be isotropic above the ocean surface.

We used the Vandaele et al. [1998] values of NO<sub>2</sub> absorption cross section and calculated the band-average values of NO<sub>2</sub> and Rayleigh scattering optical thickness for the MODIS visible and near-IR bands for our

radiative transfer calculations, following the approach described in more detail in *Ahmad et al.* [2007]. *Ahmad et al.* [2007] showed that the relative decrease in the TOA reflectance ratio due to atmospheric  $\text{NO}_2$  absorption is practically independent of the exact aerosol amount in the atmosphere. Here radiative transfer calculations were performed assuming no aerosol amount in the atmosphere. Radiative transfer calculations were performed for solar zenith angles (SZA)  $1.5^\circ$ ,  $18^\circ$ ,  $30^\circ$ ,  $42^\circ$ , and  $60^\circ$ , varying azimuth angles depending on geometry, and look angles of  $36^\circ$ ,  $42^\circ$ , and  $48^\circ$ .

Previous work has shown that the effect of  $\text{NO}_2$  on the TOA reflectance depends on the  $\text{NO}_2$  vertical distribution, with the TOA reflectance being less sensitive to increases in  $\text{NO}_2$  near the bottom boundary of the atmosphere [*Ahmad et al.*, 2007]. In the absence of measurements, air quality models can be used to predict the vertical distribution of  $\text{NO}_2$ . Radiative transfer calculations are presented here assuming homogeneous  $\text{NO}_2$  vertical distribution within the first 2 km from the ground. As discussed in section 2.4, air quality model simulations suggest that anthropogenic  $\text{NO}_2$  is primarily located within the first 2 km in the atmosphere over the Chesapeake Bay during the summertime. To show the sensitivity of TOA reflectance (and thus also error in  $R_{rs}(\lambda)$ ) to  $\text{NO}_2$  vertical profile, we also performed radiative transfer calculations for  $\text{NO}_2$  homogeneously distributed within the first 3 km from the ground.

## 2.4. Air Quality Model Simulations

We used high-resolution air quality model simulations to suggest realistic cases of trace gas vertical distribution over an estuarine environment, such as the Chesapeake Bay. The Community Multiscale Air Quality (CMAQ) [*Byun and Schere*, 2006] model was run spanning the entire DISCOVER-AQ and GeoCAPE-CBODAQ field campaigns. This model simulates anthropogenic and biogenic emissions, deposition, chemical conversion, and advective, convective, and turbulent chemical transport. CMAQ is driven by meteorological model output from the Weather Research and Forecasting (WRF) [*Skamarock et al.*, 2008] model. Anthropogenic and biomass burning emissions are fed into the model. Biogenic emissions are calculated within the CMAQ model based on land use and meteorological conditions. Lightning emissions are calculated in CMAQ based on convective precipitation as computed by WRF. Deposition is calculated in the model and is based on land use, meteorology, and how effective each pollutant is at sticking to a particular surface once it comes into contact with the surface. Air pollutants can be converted to other species through photolysis, gas-phase chemistry, aqueous chemistry, or aerosol formation/transformation processes. Horizontal and vertical pollutant transport is driven by the meteorology ingested into the model and diffusion schemes in the CMAQ model. Meteorological initial and boundary conditions for the WRF simulation came from the North American Regional Reanalysis (NARR) and chemical initial and boundary conditions for the CMAQ simulation came from the MOZART Chemical Transport Model. Additional details on how the models were set up for this simulation are found in *Loughner et al.* [2014], *Goldberg et al.* [2014], and *He et al.* [2014].

## 3. Results and Discussion

### 3.1. Measured Variability in $\text{NO}_2$ in Coastal Areas

Continuous, high temporal resolution and high-precision Pandora measurements in coastal areas near polluted urban centers revealed strong temporal and spatial gradients in  $\text{TCNO}_2$  not possible to capture by Aura-OMI alone. Ground-based observations and satellite overpass retrievals are discussed in detail below for the Chesapeake Bay estuarine environment, Helsinki on the shore of the Gulf of Finland in the Baltic Sea, and the Korean coastal megacities of Seoul and Busan along the Yellow and East Seas.

#### 3.1.1. Chesapeake Bay Estuarine Environment

Over the Eastern US Washington DC-Chesapeake Bay estuarine environment,  $\text{TCNO}_2$  varied by an order of magnitude, from 0.1 DU to 1 DU, both spatially and temporally during the DISCOVER-AQ and CBODAQ campaigns (Figures 1 and 2). Temporal variability as large as 0.5–0.8 DU within 2–4 h was measured at urban and suburban sites along the Chesapeake Bay shoreline (e.g., Essex, Old-Town, and UMCP; Figure 1). Close to urban areas,  $\text{TCNO}_2$  showed a well-defined weekly behavior, with maxima observed in the middle of the week and minimum values consistently observed over the weekend, particularly on Sundays (Figure 2, bottom). This weekly pattern was absent in relatively rural areas characterized by less traffic and lower  $\text{NO}_x$  emissions (Figure 2, top). Diurnal patterns in  $\text{TCNO}_2$  were highly variable among stations and also dependent on the day of the week. In rural areas (e.g., SERC, Fairhill, and Padonia),  $\text{TCNO}_2$  typically remained lower than 0.4 DU and varied by less than a factor of 2 without showing any consistent diurnal patterns (Figures

1a, 1e, and 2). This is consistent with 0.1–0.2 DU of  $\text{NO}_2$  residing in the stratosphere. At the urban and suburban sites, strong diurnal patterns were observed on most week-days, with maxima in  $\text{TCNO}_2$  typically occurring early in the morning and a secondary peak often observed later in the afternoon, associated with human activities and rush hour peaks in  $\text{NO}_x$  emissions (Figures 1b–1d). Peak  $\text{TCNO}_2$  often reached 1 DU, 5–10 times higher than background levels (Figure 2, bottom). A typical case of a relatively low air pollution summer week-day is shown in Figure 1 (blue solid circles), for Monday 18 July. Observed diurnal patterns in  $\text{NO}_2$  were considerably different over the weekend, when  $\text{TCNO}_2$  amounts remained below 0.5 DU at both urban and rural sites (Figure 2), with no strong diurnal variability observed. As shown in Tzortziou *et al.* [2013], the observed diurnal and day-of-the-week patterns in  $\text{NO}_2$  over the Chesapeake Bay estuarine environment are consistent with high-resolution air quality model simulations using the CMAQ model.

From a sun-synchronous polar orbit, OMI cannot capture the strong temporal variability in  $\text{NO}_2$  observed by the Pandora network and predicted by CMAQ (Figures 1 and 2). With an overpass at around 13:30 local time, OMI misses the morning and late afternoon rush hour peaks in  $\text{TCNO}_2$  observed over urban areas on most weekdays, providing a satellite image of  $\text{TCNO}_2$  corresponding to relatively low  $\text{NO}_x$  emission conditions (Figure 2). Moreover, the strong inhomogeneity in anthropogenic emissions in the Washington DC/Chesapeake Bay area results in strong spatial gradients in air quality that cannot be observed by the relatively coarse resolution measurements by OMI. The size of an OMI pixel varies with cross-track viewing zenith angle from 24 km at nadir to approximately 128 km for the extreme viewing angles of  $57^\circ$  at the edges of the swath [Boersma *et al.*, 2007]. Along the Chesapeake Bay shoreline, an area of this size includes both relatively clear rural areas as well as urban hot spots of  $\text{NO}_x$  emissions. The distance between Fairhill and GSFC (Pandora sites located the furthest apart in our network; Figure 1f) is 123 km, comparable to the size of the OMI footprint at large satellite viewing angles. Based on measurements by our Pandora network, spatial variability in  $\text{TCNO}_2$  during the DISCOVER-AQ/CBODAQ campaigns was as large as 0.7 DU within an area covered, in some cases, by just a single OMI pixel. Due to its coarse spatial resolution, OMI significantly underestimated  $\text{TCNO}_2$ , by as much as 49%, over polluted coastal urban sites, and failed to detect the high  $\text{TCNO}_2$  amounts ( $>0.4$  DU) observed by the Pandora spectrometers (Figure 2).

### 3.1.2. Helsinki, Gulf of Finland in the Baltic Sea

Total column  $\text{NO}_2$  levels were overall lower in Helsinki, Finland (Figures 3 and 4) than urban areas in the Washington-Baltimore region. Pandora measurements of  $\text{TCNO}_2$  concentrations during September 2011–April 2013 had an average of 0.24 DU (stdev = 0.11 DU), which is similar to the average  $\text{TCNO}_2$  levels measured in the relatively rural areas of the Eastern US coast (i.e., Fairhill, SERC, and Padonia). Still,  $\text{TCNO}_2$  in Helsinki reached values as high as 1.73 DU on certain occasions (Figure 4), and on some days temporal changes of more than 0.5 DU were observed within less than 3 h (Figures 1a, 1b, and 1e).

In some cases, two, or even three, OMI satellite overpass retrievals were available for the same day at this high-latitude site, providing some satellite information on  $\text{TCNO}_2$  temporal variability (e.g., Figures 3a, 3c, and 3d). Yet all OMI overpasses were from 11 am to 3 pm local time. As a result, even with three overpasses OMI was still not able to capture the strong diurnal patterns in atmospheric pollution, missing the early morning and late afternoon maxima in  $\text{TCNO}_2$  (Figure 3). Although OMI satellite retrievals were in good agreement with Pandora when  $\text{TCNO}_2$  remained lower than 0.4 DU (e.g., Figure 3), OMI failed to capture peaks in  $\text{NO}_2$  levels (Figure 4). As a result, the maximum  $\text{TCNO}_2$  measured by OMI over this coastal site was 0.6 DU, while Pandora measurements frequently exceeded 1 DU (Figure 4).

### 3.1.3. Korean Coastal Megacities, Along the Yellow and East Seas

Larger concentrations of  $\text{NO}_2$  pollution and stronger temporal gradients were measured by Pandora at the two largest cities of South Korea, Seoul and Busan (Figures 5 and 6).  $\text{TCNO}_2$  amount in Busan was on average 0.75 DU (stdev = 0.44 DU) during March 2012–March 2013, reaching as high 3.9 DU (Figure 6, bottom). Even higher  $\text{NO}_2$  amounts were measured by Pandora in the city of Seoul, with an average  $\text{TCNO}_2$  of 1.08 DU (stdev = 0.62 DU) and maximum values reaching 6 DU (Figure 6, top). Changes as large as 2.0 DU within 3–4 h were not uncommon (e.g., Figures 5b, 5d, and 5e), and in some cases  $\text{TCNO}_2$  changes as large as 3 or 4 DU during the day were recorded (Figure 6). These gradients are 3–5 times stronger than those typically observed along the US Mid-Atlantic coastal zone, or along the Helsinki coastline. Diurnal patterns were quite variable, with  $\text{NO}_2$  having maximum values some days early in the morning (Figure 5c) and some days later in the evening (Figure 5d), while in other cases showing two maxima during the day (e.g., Figures 5a and 5b).

Comparisons with Aura-OMI were in good agreement at the time of the OMI overpass and when the satellite overpass was at a small distance (<20 km) from the Pandora site (e.g., Figures 5a, 5d, and 5e). At larger satellite overpass distances, however, differences between OMI and Pandora were quite large, with OMI underestimating NO<sub>2</sub> by as much as a factor of 3 (e.g., Figure 5c). OMI was not able to capture the early morning and late afternoon peaks in TCNO<sub>2</sub> amounts (e.g., Figures 5 and 6), providing, as in the cases of Helsinki and the Eastern US coast, a satellite image of TCNO<sub>2</sub> under relatively low pollution conditions. OMI retrievals during March 2012–March 2013 showed an average TCNO<sub>2</sub> of 0.5 DU (stdev = 0.21 DU) over Busan, and 0.79 DU (stdev = 0.45 DU) over Seoul, considerably underestimating NO<sub>2</sub> pollution levels compared to the continuous observations from the Pandora spectrometers (Figure 6).

### 3.2. Error in TOA Signal From an Incorrect NO<sub>2</sub> Amount

To estimate the error in satellite-retrieved ocean remote sensing reflectance caused by not properly accounting for NO<sub>2</sub> variability during coastal ocean color atmospheric correction, we performed detailed vector radiative transfer calculations using the methods described in section 2.2.

Because a satellite OC sensor retrieves ocean color information based on the signal it measures at the top of the atmosphere, we first estimated the percent error (or change) in TOA upwelling radiance  $L_{TOA}(\lambda)$ , caused by a change of 1 DU in NO<sub>2</sub>. Radiative transfer calculations were performed for two cases: one case assuming a molecular Rayleigh atmosphere without NO<sub>2</sub> ( $L_{TOA}(\lambda)_{(NO_2=0 \text{ DU})}$ ) and a second case with NO<sub>2</sub> absorption and a total column NO<sub>2</sub> amount of 1 DU ( $L_{TOA}(\lambda)_{(NO_2=1 \text{ DU})}$ ). The percent error (or effect) in TOA signal was expressed as

$$\% \text{ error } L_{TOA}(\lambda) = \frac{L_{TOA}(\lambda)_{(NO_2=1 \text{ DU})} - L_{TOA}(\lambda)_{(NO_2=0 \text{ DU})}}{L_{TOA}(\lambda)_{(NO_2=0 \text{ DU})}} \quad (1)$$

NO<sub>2</sub> was assumed to be homogeneously distributed within the first 2 km from the ground. This is consistent with CMAQ air quality model simulations showing that most of anthropogenic pollution is distributed within the first 2 km from the ground during transport over the Chesapeake Bay and Atlantic Ocean (see also section 3.3).

As expected, the TOA upwelling radiance decreased when including atmospheric NO<sub>2</sub> absorption (Figure 7a). The error in  $L_{TOA}(\lambda)$  had a strong spectral dependence. The maximum influence, approximately 1.5% error in  $L_{TOA}(\lambda)$ , was in the 400–420 nm spectral region, consistent with the spectral shape in NO<sub>2</sub> absorption cross sections. The effect of NO<sub>2</sub> on  $L_{TOA}(\lambda)$  increased with SZA, because of the larger slant path with increasing SZA, which results in more scattering and, hence, more absorption.

### 3.3. The Effect of NO<sub>2</sub> Plume Height

Our calculations showed that the vertical distribution of NO<sub>2</sub> has a considerable impact on  $L_{TOA}(\lambda)$  (and, subsequently,  $R_{rs}$  retrievals), which is usually neglected. Simulations where 1 DU of NO<sub>2</sub> was homogeneously distributed within the first 3 km from the ground resulted in considerably larger errors, approximately 1.8% at 412 nm and SZA = 60°, compared to 1.5% error when the same TCNO<sub>2</sub> amount was distributed within the first 2 km from the ground (Figure 7b). The errors in  $L_{TOA}(\lambda)$  increased further for NO<sub>2</sub> homogeneously distributed within the first 4 km from the ground (results not shown here), suggesting that the impact of NO<sub>2</sub> on TOA signal, and as a result also on retrieved ocean  $R_{rs}$ , increases as NO<sub>2</sub> is distributed higher in the atmosphere.

We performed air quality model calculations using CMAQ to suggest realistic cases of NO<sub>2</sub> vertical distribution over the Chesapeake Bay estuary during the summertime. Results are shown in Figure 8 for four cases during July 2011. Based on the model simulations, most of the NO<sub>2</sub> over this estuarine environment is typically within the first 2 km (or, from 1000 to 800 hPa) due to anthropogenic emissions near the surface. Note that the horizontal gradient of NO<sub>2</sub> in Figure 8 has a high bias due to a high bias in anthropogenic emissions that result in a high NO<sub>2</sub> bias in urban areas [Canty *et al.*, 2013], and uncertainties in the chemistry that result in a low NO<sub>2</sub> bias over rural areas and coastal waters [Canty *et al.*, 2013]. Still, in some cases the model simulated maximum NO<sub>2</sub> over the estuarine waters (Figures 8c and 8d). On 8 July 2011, the model simulated elevated NO<sub>2</sub> concentrations aloft due to lightning (Figure 8b).

Our estimates of the impact on  $L_{TOA}$  of NO<sub>2</sub> homogeneously distributed within the 0–2 and 0–3 km layers are consistent with Ahmad *et al.* [2007], where similar radiative transfer calculations were performed, but



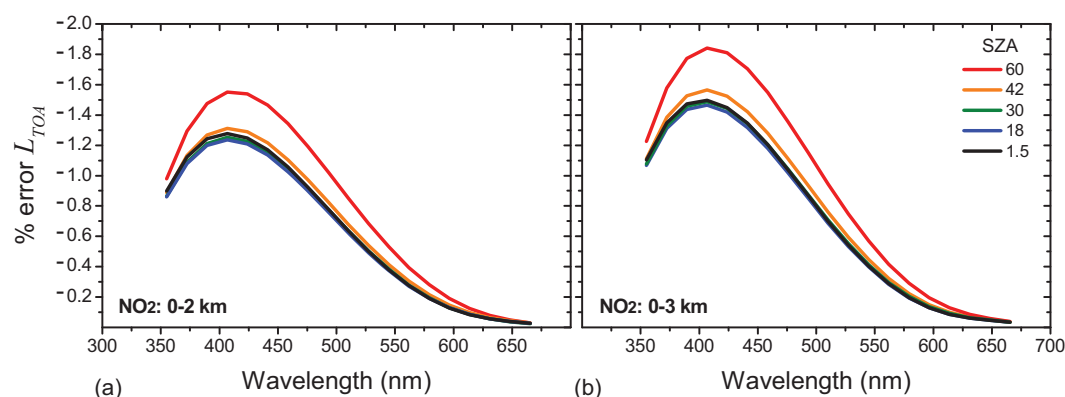


**Figure 7.** Percent error (or change) in TOA signal, caused by a change of 1 DU of  $\text{NO}_2$ , expressed as in equation (1).  $\text{NO}_2$  was assumed to be homogeneously distributed within a (a) 0–2 km layer and (b) 0–3 km layer from the ground. Results are shown here for a look angle of  $36^\circ$ , and as a function of solar zenith angle and wavelength.  $\text{NO}_2$  absorption in the atmosphere resulted in lower  $L_{\text{TOA}}$  (negative % error).

with  $\text{NO}_2$  vertical profiles constructed by combining the mean stratospheric  $\text{NO}_2$  profile obtained from the Goddard Chemical Transport Model (CTM) with a moderate-pollution tropospheric  $\text{NO}_2$  profile obtained from the Global Earth Observing System Chemistry (GEOS-CHEM) 3-D model. Consistent with our results, Ahmad *et al.* [2007] found that for a change in  $\text{NO}_2$  of  $1 \times 10^{16}$  molecules/cm (or, 0.37 DU), the error in the TOA reflectance in the blue channels of the SeaWiFS and MODIS sensors is within 0.6–0.9%, depending on SZA [Ahmad *et al.*, 2007, Figure 2].

For satellite remote sensing, determining the total column amount can be done for a spectrometer-type instrument (e.g., OMI) with spectral resolution of 0.5–0.8 nm. Determining  $\text{NO}_2$  plume height from satellite

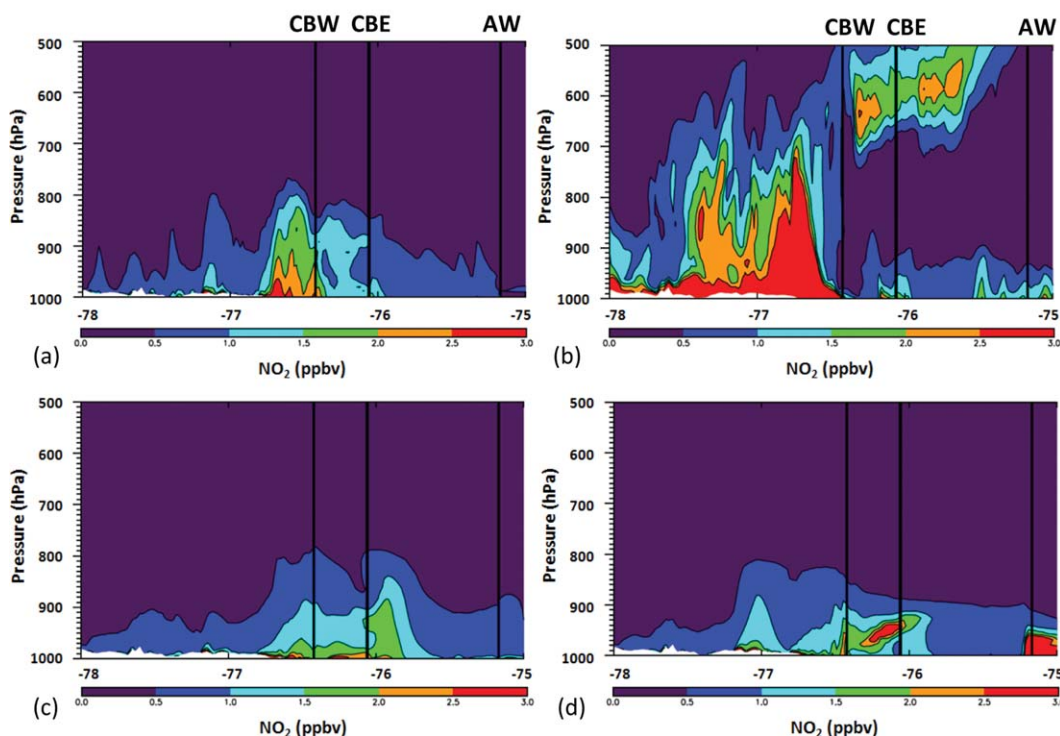


**Figure 8.** West-east cross sections of  $\text{NO}_2$  based on CMAQ simulations. The vertical lines from left to right denote the western coastline of the Chesapeake Bay (CBW), the eastern coastline of the Chesapeake Bay (CBE), and the Atlantic coastline (AW). Results are shown for 2000 UTC on (a) 7 July 2011, when  $\text{NO}_2$  showed relative homogeneous distribution within 0–2 km layer over the estuary; (b) 8 July 2011, when the model simulated  $\text{NO}_2$  at higher altitudes due to lightning; (c) 12 July 2011,  $\text{NO}_2$  distributed from 0 to 2 km layer with higher values over the estuary; (d) 29 July 2011, when the model simulated maximum  $\text{NO}_2$  over the estuary (again within 0–2 km layer).

remote sensing has not been possible for low earth orbits. If frequent observations are made from geostationary orbit, the plume motions should be detectable. The motions, combined with high-resolution model calculations should give a reasonable estimate of plume height. An alternative is measuring plume height using a ground-based spectrometer system in MaxDOAS mode, in conjunction with modeling.

### 3.4. Error in Ocean $R_{rs}$ Due to Unaccounted Variability in $\text{NO}_2$

For space-based retrievals of ocean color, any unaccounted  $\text{NO}_2$  amount and variability in the atmosphere will result in observed changes in the TOA upwelling radiance  $L_{TOA}(\lambda)$ , which will appear to be caused by the water-leaving radiance contribution. The relative error in satellite-retrieved water-leaving radiance  $L_w(\lambda)$  (or, similarly, in ocean remote sensing reflectance  $R_{rs}(\lambda)$ ) caused by 1 DU error in atmospheric  $\text{NO}_2$  can be estimated based on the relationship between  $L_{TOA}(\lambda)$  and  $L_w(\lambda)$ . Following the radiative transfer theory, with transmittance  $t$  through the atmosphere and neglecting for simplicity the glint and white cap contributions since these are assumed to be constant here, we have

$$L_{TOA}(\lambda) = tL_w(\lambda) + L_{atm}(\lambda) \quad (2)$$

For a change at the TOA due a change in water-leaving radiance, we have

$$L_{TOA}(\lambda)' = tL_w(\lambda)' + L_{atm}(\lambda) \quad (3a)$$

$$\frac{L_{TOA}(\lambda) - L_{TOA}(\lambda)'}{L_{TOA}(\lambda)} = \frac{t(L_w(\lambda) - L_w(\lambda)')}{L_{TOA}(\lambda)} \quad (3b)$$

$$\frac{\Delta L_{TOA}(\lambda)}{L_{TOA}(\lambda)} = t \frac{L_w(\lambda)}{L_{TOA}(\lambda)} \frac{\Delta L_w(\lambda)}{L_w(\lambda)} \quad (3c)$$

Based on the above and using the radiative transfer code to calculate the quantity  $t \frac{L_w(\lambda)}{L_{TOA}(\lambda)}$ , we estimated the relative error in satellite-retrieved  $L_w(\lambda)$  (or,  $R_{rs}(\lambda)$ ) in the case that a change in  $L_{TOA}(\lambda)$  (due to a change in  $\text{NO}_2$ ) is wrongfully attributed to a change in the water-leaving radiance contribution. Results for SZAs in the range  $1.5^\circ$ – $60^\circ$ , and a look angle of  $36^\circ$  are shown in Figure 9 for  $\text{NO}_2$  homogeneously distributed within 0–2 km (Figure 9a) and 0–3 km (Figure 9b) layer. As in the case of  $L_{TOA}(\lambda)$ , the percent error in ocean  $R_{rs}$  was expressed as

$$\% \text{ error } R_{rs}(\lambda) = \frac{R_{rs}(\lambda)_{(\text{NO}_2 = 1 \text{ DU})} - R_{rs}(\lambda)_{(\text{NO}_2 = 0 \text{ DU})}}{R_{rs}(\lambda)_{(\text{NO}_2 = 0 \text{ DU})}} \quad (4)$$

As expected, the ocean  $R_{rs}$  will be underestimated when there is some amount of unaccounted  $\text{NO}_2$  absorption in the atmosphere, because the decrease in the TOA signal will be incorrectly attributed to a lower ocean  $R_{rs}$ . In optically thick, strongly absorbing estuarine and coastal waters, the contribution of the water-leaving radiance to the TOA signal is typically less than 5% and can be as low as 1% [IOCCG, 2010]. In our calculations for a typical case in the Chesapeake Bay estuarine environment, the contribution of  $L_w$  to the  $L_{TOA}$  was 2.5% at 412 nm and  $\text{SZA} = 30^\circ$ . As a result and based on equation (3c), an underestimation in  $L_{TOA}(412)$  by approximately 1.3% due to 1 DU of unaccounted atmospheric  $\text{NO}_2$  (Figure 7a) corresponds to a large underestimation in ocean  $R_{rs}(412)$  by 60% at  $30^\circ$  SZA and  $\text{NO}_2$  distributed within the first 2 km from the ground (Figure 9a).

The error in ocean  $R_{rs}$  increases with solar zenith and look angles, because the error in  $L_{TOA}$  increases with increasing optical path, and also the relative contribution of ocean water-leaving radiance to the TOA signal decreases with increasing solar zenith and look angles (Figures 9a and 10). Moreover, the error in ocean  $R_{rs}$  is spectrally dependent due to the spectral dependence of the quantity  $t \frac{L_w(\lambda)}{L_{TOA}(\lambda)}$ . The error becomes even larger in the 350–400 nm spectral range (Figure 9), wavelengths that we expect to have in future OC sensors such as the polar orbiting PACE (Preaerosol, Clouds and ocean Ecosystem), and the planned geostationary sensors GEO-CAPE and GOCI-II [Ahn, 2011; Fishman et al., 2012; PACE Science Definition Team, 2012]. Our radiative transfer calculations show that the error in satellite-retrieved ocean  $R_{rs}(412)$ , caused by 1 DU unaccounted variability (temporal or spatial) in  $\text{NO}_2$  during atmospheric correction, can be as large as 70–100% for SZAs in the  $42$ – $60^\circ$  range (expected to have with a geostationary sensor such as GEO-CAPE) and for  $\text{NO}_2$  homogeneously distributed within the first 2 km from the ground (Figure 10). As in the case of the error in  $L_{TOA}$ , the error in ocean  $R_{rs}$  gets larger if some of the  $\text{NO}_2$  is distributed at higher altitudes in the atmosphere (Figure 9b).

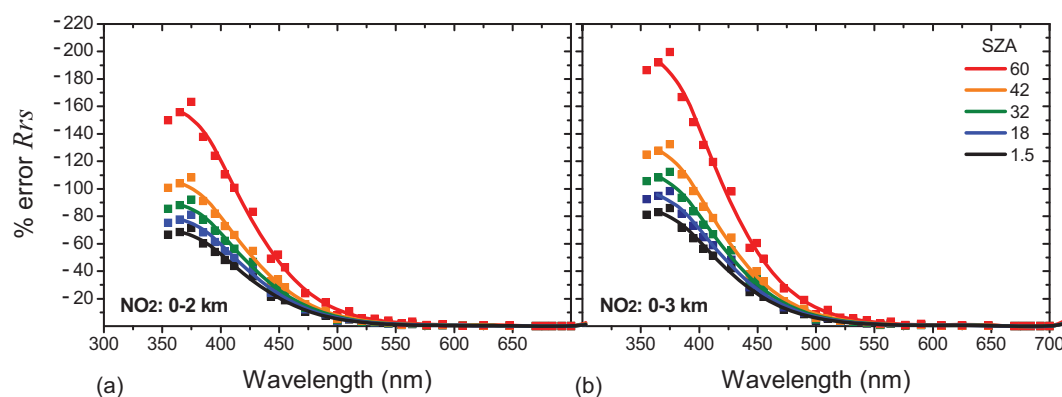


**Figure 9.** Percent error in ocean remote sensing reflectance,  $R_{rs}$ , caused by neglecting 1 DU of  $\text{NO}_2$  homogeneously distributed within a (a) 0–2 km layer and (b) 0–3 km layer from the ground. The unaccounted absorption in the atmosphere resulted in an underestimation in retrieved ocean  $R_{rs}$  (negative error). Results are shown here for a look angle of  $36^\circ$ , and as a function of solar zenith angle and wavelength. Radiative transfer calculations were performed assuming water composition typical of optically thick coastal waters, with  $L_w/L_{\text{TOA}} = 2.5\%$  at 412 nm and  $\text{SZA} = 30^\circ$ .

The implications of these errors in  $R_{rs}$  for ocean color retrievals are discussed below, in context with atmospheric  $\text{NO}_2$  variability typically measured by ground-based Pandora instruments located in moderately to highly polluted coastal urban areas. The errors for satellite-retrieved in-water biogeochemical variables were calculated using NASA OC algorithms for standard  $Chl a$  products and peer-reviewed published retrievals for CDOM.

### 3.5. Error in Satellite-Retrieved Chlorophyll-a Due to Atmospheric $\text{NO}_2$

The suite of  $Chl a$  ( $\text{mg}/\text{m}^3$ ) algorithms used in operational processing of ocean color data from sensors such as SeaWiFS, MODIS, OCTS, and VIIRS, are polynomial best fits that relate log-transformed  $Chl a$  values to log-transformed ratios of satellite-measured remote sensing reflectance at specific wavelengths  $\lambda_1$  and  $\lambda_2$ , according to

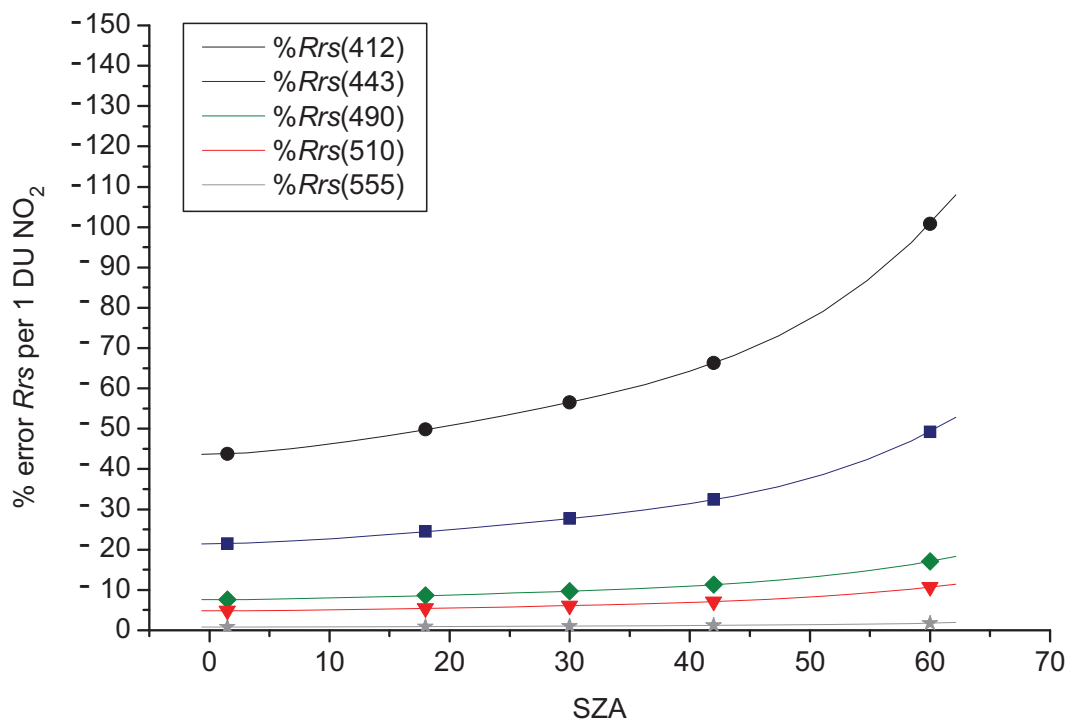


**Figure 10.** Percent error in  $R_{rs}(\lambda_o)$  as a function of SZA caused by not accounting for 1 DU of atmospheric  $\text{NO}_2$ . Results are shown here for  $\lambda_o = 412$  nm (circles),  $\lambda_o = 443$  nm (squares),  $\lambda_o = 490$  nm (diamonds),  $\lambda_o = 510$  nm (triangles), and  $\lambda_o = 555$  nm (asterisks). The unaccounted  $\text{NO}_2$  absorption in the atmosphere resulted in an underestimation in retrieved ocean  $R_{rs}$  (negative error).

$$Chla = 10^{a_0 + a_1 x + a_2 x^2 + a_3 x^3 + a_4 x^4} \quad (5)$$

where

$$x = \log_{10} \left[ \frac{R_{rs}(\lambda_1)}{R_{rs}(\lambda_2)} \right] \quad (6)$$

The wavelengths and polynomial coefficients used in operational MSI2 processing are provided on NASA's Ocean Color Forum website (<http://oceancolor.gsfc.nasa.gov/forum/>) for various algorithms, including the SeaWiFS OC4 and OC3S and OC2S, the MODIS OC3M and OC2M(-HI), the OCTS OC40, the CZCS OC3C, the MERIS OC4E, and the VIIRS OC3V.

Here we used the MODIS OC3M *Chla* algorithm to estimate the error in satellite-retrieved *Chla* due to unaccounted variability in atmospheric NO<sub>2</sub> absorption. Similar results would be obtained using other *Chla* algorithms, or updated/revised retrievals. The SeaWiFS-analog OC3M algorithm (used for the operational MODIS level-2 standard *Chla* product "Chlor-a") is an empirical algorithm (fourth-order polynomial) that relates the greater of the ratios  $R_{rs}(443)/R_{rs}(551)$  or  $R_{rs}(488)/R_{rs}(551)$  to *Chla* concentration. Because the error of any unaccounted atmospheric NO<sub>2</sub> on  $L_{TOA}$  and  $R_{rs}$  is spectrally dependent, it would affect the comparison of the above  $R_{rs}$  ratios (in a different way for different solar zenith and look angles, or changes in NO<sub>2</sub> vertical distribution), and could result in using the wrong  $R_{rs}$  ratio in the OC3M *Chla* retrieval. For example, an area with ocean  $R_{rs}(443) > R_{rs}(488)$  could falsely appear having  $R_{rs}(443) < R_{rs}(488)$  under high atmospheric NO<sub>2</sub> conditions. Since in this study our radiative transfer calculations were made for optically complex coastal waters where  $R_{rs}(488)$  is typically greater than  $R_{rs}(443)$ , we discuss mainly errors in *Chla* concentrations based on the  $R_{rs}(488)/R_{rs}(551)$  ratio. Errors in *Chla* retrievals based on the use of the  $R_{rs}(443)/R_{rs}(551)$  band ratio are much larger and are shown in Figure 11 for comparison. The polynomial coefficients we used for equation (5) are  $a = [0.2830, -2.753, 1.457, 0.659, -1.403]$ , based on O'Reilly *et al.* [2000].

The impact of a constant error in atmospheric NO<sub>2</sub> amount on the absolute magnitude and diurnal behavior of  $L_{TOA}(\lambda)$ ,  $R_{rs}(\lambda)$ , and *Chla* was estimated for  $\Delta NO_2 = 0.7$  DU (Figure 11). Such an error in TCNO<sub>2</sub> is of the order of the temporal and spatial variability, we observed with the Pandora network (but not captured by the coarser resolution OMI) in the Chesapeake Bay estuarine environment and consistent with the temporal variability often measured by Pandora in Helsinki (Figures 1–4). It is also considerably smaller than the diurnal changes typically observed at the Korean coastal cities of Seoul and Busan, where TCNO<sub>2</sub> often varied by 2.0 DU within 3–4 h (Figures 5 and 6).

The impact of such an error in TCNO<sub>2</sub> on the TOA signal and, consequently, on  $R_{rs}$  and *Chla*, was estimated as a function of time, for Lat = 40°N and 21 June (summer solstice). As expected (Figure 9), any unaccounted atmospheric NO<sub>2</sub> absorption results in an underestimation of  $R_{rs}$ , more so at 443 and 488 nm than at 551 nm, subsequently resulting in an underestimation of the  $R_{rs}(443)/R_{rs}(551)$  and  $R_{rs}(488)/R_{rs}(551)$  ratios, and an overestimation of *Chla* concentration (Figure 11). A false diurnal pattern was retrieved for *Chla*, with maxima in the morning and afternoon corresponding to increased NO<sub>2</sub> absorption (larger error) at larger solar zenith angles. This apparent diurnal change in *Chla* does not correspond to any real variability in water bio-optical properties or atmospheric composition. *Chla* errors, using the  $R_{rs}(488)/R_{rs}(551)$  ratio and assuming NO<sub>2</sub> within a 0–2 km layer, were 20% for small SZAs around noon and increased to >50% for retrievals at SZAs > 60° (Figure 11, left). Use of the  $R_{rs}(443)/R_{rs}(551)$  ratio would result in errors as large as 70% at noon and larger than 200% in the early morning and late afternoon (Figure 11, right). The error becomes larger if we assume a 3 km NO<sub>2</sub> layer (Figure 11).

Any temporal variability in the atmospheric total column NO<sub>2</sub> amount or vertical distribution during the day (e.g., see Figures 1, 3, and 5) would also result in a false temporal variability in *Chla*, in addition to the false diurnal pattern due to the proportionally larger error of a certain amount of NO<sub>2</sub> at large SZAs (Figure 13). Such a false temporal variability in *Chla* would be impossible to distinguish from any actual temporal patterns in coastal ocean dynamics without measurements of NO<sub>2</sub> temporal variability over the site of interest.

### 3.6. Error in Retrieved CDOM From an Incorrect NO<sub>2</sub> Amount

Satellite retrievals of CDOM absorption are based on both semianalytical models that simultaneously retrieve water inherent optical properties (e.g., CDOM and detrital absorption  $a_{CDM}$ , phytoplankton absorption  $a_{phytr}$ , particulate backscattering  $b_b$ ) from the ocean  $R_{rs}$  spectra, as well as empirical relationships relating CDOM absorption to  $R_{rs}$  ratios of various OC bands [e.g., Johannessen *et al.*, 2003; Doxaran *et al.*, 2005;



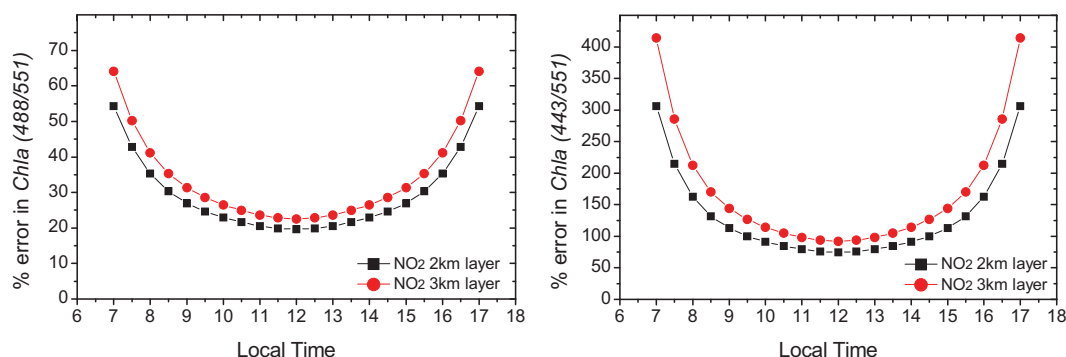


**Figure 11.** False diurnal variability in  $Chla$  (error shown in %) due to a constant error in  $NO_2$  of 0.7 DU, (left) using the 488/551 band ratio and (right) using the 443/551 band ratio for  $Chla$  retrievals. Results are shown for  $NO_2$  homogeneously distributed within the first 2 km (squares) and within the first 3 km (circles) from the ground.

Tehrani et al., 2013; Le and Hu, 2013]. Almost all of these retrievals use  $R_{rs}$  in the 412–490 spectra region to retrieve CDOM absorption and spectral slope and link to DOC dynamics. D'Sa and Miller [2003] found that  $R_{rs}(412)/R_{rs}(510)$  is the optimal band ratio for CDOM retrievals for the Mississippi River plume environment. However, they observed larger CDOM absorption retrieval errors for this ratio compared to using  $R_{rs}$  at 443 and 490, which they attributed partly to errors in atmospheric correction. This is consistent with our results in Figure 9.

Kahru and Mitchell [2001] used the SeaWiFS  $R_{rs}(443)/R_{rs}(510)$  ratio to retrieve  $a_{CDOM}(300)$  at the CalCOFI site in southern California. Using measurements from the US Mid Atlantic Bight (area extending from the Delaware Bay mouth to the region south of the Chesapeake Bay mouth), Mannino et al. [2008] developed empirical algorithms to retrieve CDOM absorption at 355, 412, and 443 nm from the MODIS-Aqua bands  $R_{rs}(490)/R_{rs}(551)$  and the SeaWiFS bands  $R_{rs}(490)/R_{rs}(555)$  [Mannino et al., 2008, Table 1]. From these CDOM absorption coefficients, they then estimated the CDOM absorption spectral slope  $S_{CDOM}$ . They also derived dissolved organic carbon (DOC) concentration based on seasonal and regionally specific relationships between  $a_{CDOM}(355)$  and DOC [Mannino et al., 2008]. Here we estimated the error in satellite-retrieved CDOM due to unaccounted absorption by atmospheric  $NO_2$ , using the CDOM retrievals derived by Mannino et al. [2008] and Kahru and Mitchell [2001]. A similar approach can be used to estimate errors in CDOM based on other published and updated CDOM retrieval algorithms.

Mannino et al. [2008] used a nonlinear one-phase exponential decay regression model to relate  $R_{rs}$  to CDOM absorption and derived  $a_{CDOM}$  from the equation

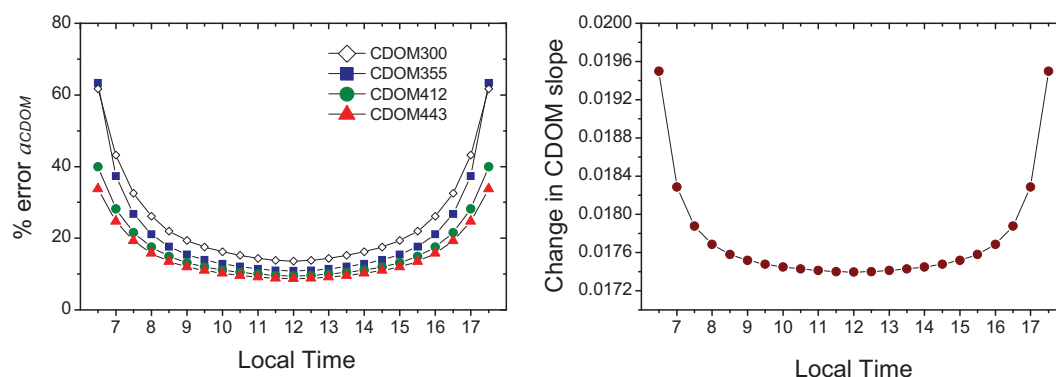


**Figure 12.** (left) False diurnal variability (%) in retrieved CDOM absorption for constant error in  $NO_2$  of 0.7 DU, assuming homogeneous distribution of  $NO_2$  in the 0–2 km layer. CDOM absorption coefficients are shown at 300 nm, using the Kahru and Mitchell [2001] algorithm, and at 355, 412, and 443 nm, using the MODIS-Aqua CDOM retrievals proposed by Mannino et al. [2008]; (right) resulting false diurnal change in CDOM absorption spectral slope  $S_{CDOM}$ , based on Mannino et al. [2008].

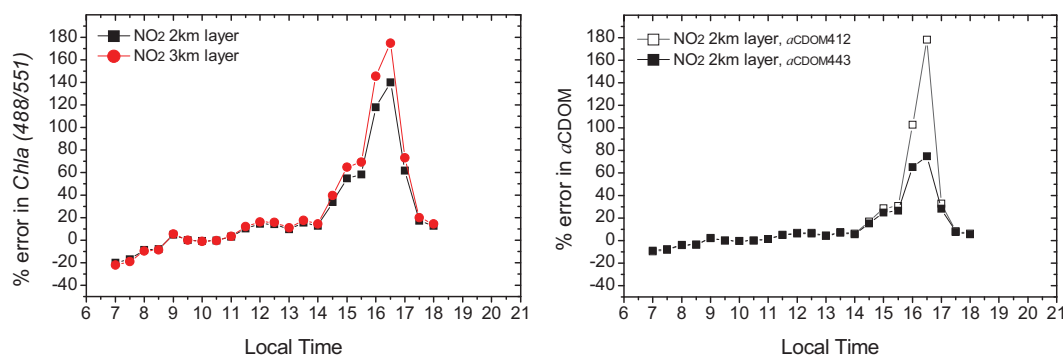


**Figure 13.** (left) False diurnal variability (%) in retrieved *Chla* (using the 488/551 band ratio) due to unaccounted variability in  $\text{NO}_2$  for the case of Busan, 30 March 2012 (see Figure 5d). OMI on this day measured 0.75 DU during its overpass time, while  $\text{TCNO}_2$  measured by Pandora varied from 0.4 to 2.4 DU. Results are shown for  $\text{NO}_2$  homogeneously distributed within the first 2 km (squares) and within the first 3 km (circles) from the ground. (right) False diurnal variability (%) in retrieved CDOM absorption (412 and 443 nm) for the same case, assuming homogeneous distribution of  $\text{NO}_2$  within 0–2 km.

$$a_{\text{CDOM}}(\lambda) = \ln \left[ \frac{R_{rs} \text{ratio} - a}{b} \right] / (-c) \quad (7)$$

where  $R_{rs} \text{ ratio}$  is  $R_{rs}(490)/R_{rs}(555)$  for SeaWiFS and  $R_{rs}(490)/R_{rs}(551)$  for MODIS-Aqua. For MODIS-Aqua retrievals, the coefficients  $[a, b, c]$  are  $[0.4934, 2.731, 3.512]$ ,  $[0.4553, 2.345, 8.045]$ , and  $[0.4363, 2.221, 13.126]$  for  $a_{\text{CDOM}}$  at 355, 412, and 443, respectively. For SeaWiFS retrievals, these coefficients are  $[0.4847, 3.055, 3.642]$ ,  $[0.4443, 2.599, 8.327]$ , and  $[0.4247, 2.453, 13.586]$  for  $a_{\text{CDOM}}$  at 355, 412, and 443, respectively.

We used equation (7) and the coefficients for MODIS-Aqua to retrieve CDOM from our measured ocean  $R_{rs}$  spectra assuming no error in atmospheric correction for  $\text{NO}_2$ , and also from the false  $R_{rs}$  spectra derived after assuming a constant error in  $\text{NO}_2$  throughout the day with  $\Delta\text{NO}_2 = 0.7$  DU and homogeneous distribution of  $\text{NO}_2$  in the 0–2 km layer. Results are shown in Figure 12 for  $a_{\text{CDOM}}$  at 355, 412, and 443. Calculations were performed for  $\text{Lat} = 40^\circ\text{N}$  and the summer solstice. Similarly to the *Chla* retrievals, a false diurnal variability was retrieved for CDOM with maximum retrieval errors at large SZAs in the morning and in the afternoon. CDOM errors were as large as 25–30% for retrievals at 443 nm and increased with decreasing wavelength reaching 40–60% for CDOM retrievals at 355 nm. These errors in CDOM spectral absorption coefficients affected retrievals of the CDOM absorption spectral slope, with  $S_{\text{CDOM}}$  showing an apparent change during the day from more than  $0.019 \text{ nm}^{-1}$  in the morning to almost  $0.0174 \text{ nm}^{-1}$  at noon (Figure 12, right).

CDOM errors of similar magnitude were estimated using the *Kahru and Mitchell* [2001] approach that relates  $a_{\text{CDOM}}$  at 300 nm to the SeaWiFS OC bands 443/510, according to

$$a_{\text{CDOM}}(\lambda) = 10^{a_0 + a_1 x} \quad (8)$$

where  $x = \log_{10} \left[ \frac{L_{\text{wn}}(443)}{L_{\text{wn}}(510)} \right]$ , and the coefficients  $[a_0, a_1]$  are  $[-0.393, -0.872]$ . A false diurnal variability in CDOM was derived, with errors in retrieved CDOM absorption at 300 nm as large as 40–60% (Figure 12, left).

As in the case of *Chla*, errors in retrievals of CDOM optical properties would be higher for  $\text{NO}_2$  distributed at higher altitudes. Any change in the total column amount or vertical distribution of atmospheric  $\text{NO}_2$  during the day would result in additional false retrieval of temporal variability in CDOM absorption magnitude and spectral shape (Figure 13, right).

#### 4. Summary and Conclusions

As the consequences of increasing coastal urbanization and climate variability are becoming more profound, improving space-based monitoring of carbon, nutrient, and pollutants in nearshore waters becomes increasingly important for understanding impacts of environmental change on coastal ecosystem dynamics,

biology, biogeochemistry, and biodiversity. Despite the recent development of increasingly sophisticated satellite bio-optical algorithms, monitoring nearshore biogeochemical processes from space remains a major challenge, partly due to the high (and often unaccounted) variability in coastal air pollution.

As reported by the EPA's National Emissions Inventory (NEI), NO<sub>x</sub> emissions in the US have been reduced nationwide by 38% between 2002 and 2011 [Loughner *et al.*, 2013]. This has been achieved through a combination of (1) the Environmental Protection Agency (EPA) NO<sub>x</sub> State Implementation Plan (SIP) call, which required 22 states and the District of Columbia to regulate NO<sub>x</sub> emissions to mitigate ozone transport, (2) the NO<sub>x</sub> Budget Trading Program, and (3) subsequent EPA rules, court orders, and state regulations [Loughner *et al.*, 2013]. Despite these significant reductions in NO<sub>x</sub> emissions since 2002, we measured total column NO<sub>2</sub> amounts of 1 DU during our 2011 field campaign in the Chesapeake Bay region. Previous studies discussing longer time series observations from the Pandora spectrometers at the GSFC site, covering various seasons and multiple years, reported even larger variability in NO<sub>2</sub> with total column amounts in the range 0.2–2 DU [Herman *et al.*, 2009]. In urban and suburban regions along the Chesapeake Bay shoreline, we found clear diurnal and day-of-the-week patterns in NO<sub>2</sub>, associated with rush hour emissions. Temporal variability in NO<sub>2</sub> during our measurements was as large as 0.5–0.8 DU within 2–4 h, while spatial variability was as large as 0.7 DU within an area covered, in some cases, by just a single OMI pixel.

Weak regulation of anthropogenic emissions in newly industrialized and developing countries often result in poor air quality conditions. TCNO<sub>2</sub> in the Korean coastal cities of Seoul and Busan, was significantly larger than in the US or in Europe. We measured TCNO<sub>2</sub> amounts as high as 3.9 DU in Busan, while maximum TCNO<sub>2</sub> reached 6 DU in Seoul. Changes as large as 2.5 DU within 3–4 h were not uncommon, and in some cases TCNO<sub>2</sub> changes as large as 3 or 4 DU during the day were recorded. With coarse spatial resolution and an overpass at around 13:30 local time, OMI cannot detect the strong spatial and temporal variability we observed in NO<sub>2</sub> over coastal urban areas in North America, Europe, and Asia, missing pollution peaks from industrial and rush hour activities. As a result, daily retrievals and monthly climatology from OMI provide satellite NO<sub>2</sub> distributions that considerably underestimate near-urban coastal pollution levels compared to continuous ground-based observations (Figures 2, 4, and 6).

To account for the known strong NO<sub>2</sub> variability in coastal ocean color retrievals requires measurements of NO<sub>2</sub> at a spatial and temporal resolution relevant to the satellite ocean color observations. For ocean color measurements from polar orbit satellite sensors, nearly coincident satellite NO<sub>2</sub> measurements would be required to capture the diurnal variability in NO<sub>2</sub> associated with rush hour emissions. For example, the MODIS-Terra overpass time (daytime mode at the equator) is around 10:30 local solar time, coinciding approximately with the maximum in TCNO<sub>2</sub> over coastal urban areas, while the MODIS-Aqua overpass time is around 13:30 local solar time. High-spatial and temporal resolution retrievals of atmospheric NO<sub>2</sub> are even more critical for geostationary ocean color measurements, to avoid aliasing atmospheric variability for diurnal changes or spatial gradients in ocean composition. Our radiative transfer calculations showed that 0.7 DU unaccounted variability in NO<sub>2</sub>, which is consistent with the spatial and temporal variability we observed in TCNO<sub>2</sub> over our coastal sites, results in an error in coastal water  $R_{rs}(412)$  as large as 40% at low SZAs (<30°), while it gets as large as 70–80% for large SZAs expected to have with a geostationary sensor. The error in  $R_{rs}$  gets larger at shorter wavelengths (350–400 nm), at larger solar zenith and look angles, and as the NO<sub>2</sub> is distributed at higher altitudes. The resulting errors in coastal water  $R_{rs}$  subsequently affect retrievals of coastal ocean biogeochemical variables from space.

A number of previous studies [Ruddick *et al.*, 2001; Gitelson *et al.*, 2007; Tzortziou *et al.*, 2007; Le *et al.*, 2013] highlighted and demonstrated the advantages of using red-green wavelengths, instead of information in the blue spectral region, for improved *Chla* retrievals in estuarine and coastal waters. Yet current operational retrievals for standard *Chla* products (e.g., MODIS OC3M) are based on empirical relationships between *Chla* and  $R_{rs}$  at blue wavelengths (e.g., 443 and 490 nm) that are considerably affected by errors in atmospheric NO<sub>2</sub>. Even if wavelengths in the spectral range affected by NO<sub>2</sub> absorption (i.e., 330–490 nm) are not used for *Chla* retrievals, this UV-visible spectral region is critical for retrievals of CDOM and DOC dynamics both from current and future, hyperspectral and multichannel, satellite ocean color sensors [e.g., Mannino *et al.*, 2008; Le and Hu, 2013]. Using current operational and published algorithms for *Chla* and CDOM, we estimated the implications of these errors in  $R_{rs}$  for satellite retrievals of ocean biogeochemical variables. A constant error in NO<sub>2</sub> of 0.7 DU throughout the day resulted in a false variability in *Chla* and CDOM, with errors reaching 40–60% for *Chla* retrievals using the 488/551 band ratio. Errors in retrieved CDOM spectral absorption coefficients were as large as 40–60% and affected retrievals of the CDOM absorption spectral slope, an optical

parameter often used to understand changes in the origin, quality, and composition of CDOM.  $S_{CDOM}$  showed an apparent diurnal change from more than  $0.019 \text{ nm}^{-1}$  early in the morning to almost  $0.017 \text{ nm}^{-1}$  at noon. These errors in CDOM are larger (and in the case of  $S_{CDOM}$  in opposite direction) than reported changes in CDOM absorption properties during photochemical degradation experiments where CDOM was exposed to natural sunlight over a period of several days [e.g., Tzortziou et al., 2007; Osburn et al., 2001].

It should be noted that the observed variability in  $\text{TCNO}_2$  is based on measurements at coastal sites over the land. If we assume a smaller error in  $\text{TCNO}_2$  over coastal waters, for example, due to pollutants dispersion and  $\text{NO}_2$  chemical transformation, the errors in coastal ocean retrievals would be expected to be lower. However, recent studies have shown that development of bay-breeze or sea-breeze circulation can result in accumulation and buildup of atmospheric pollutants over an estuary or coastal waters [Loughner et al., 2011, 2014]. Moreover, certain meteorological conditions favor the development of strong and prolonged bay-breeze events that result in transport of a large amount of urban air pollution to higher altitudes where pollutants have longer lifetime and are susceptible to long-range transport offshore and over adjacent ocean environments [Loughner et al., 2014]. Radiative transfer calculations show that  $\text{NO}_2$  at higher altitudes have a proportionally larger impact on TOA reflectance, resulting in larger errors in water  $R_{rs}$  and biogeochemical variables. Lightning emissions can also result in larger  $\text{NO}_2$  variability at higher altitudes, increasing errors in TOA reflectance, ocean  $R_{rs}$ ,  $Chla$ , CDOM, and other bio-optical retrievals. Even larger errors than 0.7 DU in  $\text{TCNO}_2$  are expected in urban coastal areas of developing countries. In the coastal cities of Seoul and Busan, changes in  $\text{TCNO}_2$  as large as 2 DU within 3–4 h were not uncommon. If not adequately corrected, this temporal variability in  $\text{TCNO}_2$  would significantly affect the accuracy of satellite retrievals of coastal ocean color and biogeochemistry in the Yellow and East Seas. This is particularly critical for the geostationary GOCI and GOCI-II satellite missions that aim at providing high-resolution observations of coastal ocean dynamics and ecosystem processes around the Korean peninsula.

More measurements are needed over aquatic environments, to improve understanding and modeling of atmospheric  $\text{NO}_2$  variability, spatial gradients, and vertical distribution, and accurately account for  $\text{NO}_2$  absorption in satellite and aircraft remote sensing retrievals of optical and biogeochemical variables in lakes, estuaries, and coastal waters near polluted urban areas.

# Acknowledgments

This work was supported under the National Aeronautics and Space Administration (NASA) DISCOVER-AQ project (grant NNX10AR39G) and the NASA CBODAQ field campaign, with additional support from grants NASA.NNX10AQ79G and NASA.NNX11AP07G. The authors would like to thank Christian Retscher, James H. Crawford, Kenneth E. Pickering, Antonio Mannino, Jhoon Kim, Jae Kim, Jari Hovila, Johanna Tamminen, and two anonymous reviewers for their constructive comments and suggestions for improvement of the manuscript. The Pandora data are publicly available on NASA's AVDC (Aura Validation Data Center) site (<http://avdc.gsfc.nasa.gov/>).

# References

- Ahmad, Z., and R. S. Fraser (1982), An iterative radiative transfer code for ocean-atmosphere systems, *J. Atmos. Sci.*, **39**, 656–665.
- Ahmad, Z., C. R. McClain, J. R. Herman, B. Franz, E. Kwiatkowska, W. Robinson, E. J. Bucsela, and M. Tzortziou (2007), Atmospheric correction for  $\text{NO}_2$  absorption in retrieving water-leaving reflectances from the SeaWiFS and MODIS measurements, *Appl. Opt.*, **46**(26), 6504–6512.
- Ahn, Y. H. (2011), Korean GOCI status and GOCI-II development plans, in *GEO-CAPE Community Workshop*, National Center for Atmospheric Research (NCAR), Boulder, Colo. [Available at <http://geo-cape.larc.nasa.gov/events-MAY2011CW-presentations.php>.]
- Beirle, S., U. Platt, R. von Glasow, M. Wenig, and T. Wagner (2004), Estimate of nitrogen oxide emissions from shipping by satellite remote sensing, *Geophys. Res. Lett.*, **31**, L18102, doi:10.1029/2004GL020312.
- Boersma, K. F., E. Bucsela, E. Brinksma, and J. F. Gleason (2002),  $\text{NO}_2$ , in *Algorithm Theoretical Baseline Document: OMI Trace Gas Algorithms, ATBD-OMI-04*, Version 2.0, vol. IV, edited by K. Chance, 78 p., Smithsonian Astrophys. Obs., Cambridge, Mass.
- Boersma, K. F., H. J. Eskes, E. W. Meijer, and H. M. Kelder (2005), Estimates of lightning  $\text{NO}_x$  production from GOME satellite observations, *Atmos. Phys. Chem.*, **5**, 2311–2331.
- Boersma, K. F., et al. (2007), Near-real time retrieval of tropospheric  $\text{NO}_2$  from OMI, *Atmos. Chem. Phys.*, **7**(8), 2103–2118.
- Boersma, K. F., D. J. Jacob, H. J. Eskes, R. W. Pinder, J. Wang, and R. J. van der A (2008), Inter-comparison of SCIAMACHY and OMI tropospheric  $\text{NO}_2$  columns: Observing the diurnal evolution of chemistry and emissions from space, *J. Geophys. Res.*, **113**, 1–14, doi:10.1029/2007JD008816.
- Bovensmann, H., J. P. Burrows, M. Buchwitz, J. Frerick, S. Noel, V. V. Rozanov, K. V. Chance, and A. P. H. Goede (1999), SCIAMACHY: Mission objectives and measurement modes, *J. Atmos. Sci.*, **56**(2), 127–150.
- Burrows, J. P., et al. (1999), The global ozone monitoring experiment (GOME): Mission concept and first scientific results, *J. Atmos. Sci.*, **56**(2), 151–175.
- Bucsela, E. J., E. A. Celarier, M. O. Wenig, J. F. Gleason, J. P. Veefkind, K. F. Boersma, and E. J. Brinksma (2006), Algorithm for  $\text{NO}_2$  vertical column retrieval from the Ozone Monitoring Instrument, *IEEE T. Geosci. Remote*, **44**, 1245–1258, doi:10.1109/tgrs.2005.863715.
- Byun, D., and K. L. Schere (2006), Review of the governing equations, computational algorithms, and other components of the Models-3 Community Multiscale Air Quality (CMAQ) modeling system, *Appl. Mech. Rev.*, **59**, 51–77.
- Callies, J., E. Corpaccioli, M. Eisinger, A. Hahne, and A. Lefebvre (2000), GOME-2: Metop's second generation sensor for operational ozone monitoring, *ESA Bull.*, **102**, 28–36.
- Canty, T., et al. (2013), Improving air quality models through the use of satellite retrievals and aircraft observations, in *Biannual Meeting on NASA Air Quality Applied Sciences Team*, 5 Jun. University of Maryland, College Park, Md. [Available at [http://acmg.seas.harvard.edu/presentations/aqast/jun2013/day2\\_pm/5\\_canty\\_aqast\\_5june\\_final.pdf](http://acmg.seas.harvard.edu/presentations/aqast/jun2013/day2_pm/5_canty_aqast_5june_final.pdf).]
- Carder, K. L., F. R. Chen, Z. Lee, S. K. Hawes, and J. P. Cannizzaro (2003), Case 2 Chlorophyll a. MODIS ocean science team algorithm theoretical basis document, *ATBD 19*, pp. 1–67, Coll. of Mar. Sci., Univ. of South Fla., St. Petersburg, Fla.
- Cede, A., J. Herman, A. Richter, N. Krotkov, and J. Burrows (2006), Measurements of nitrogen dioxide total column amounts at Goddard space flight center using a brewer spectrometer in direct sun mode, *J. Geophys. Res.*, **111**, D05304, doi:10.1029/2005JD006585.



- Celarié, E. A., et al. (2008), Validation of ozone monitoring instrument nitrogen dioxide columns, *J. Geophys. Res.*, **113**, D15S15, doi:10.1029/2007JD008908.
- Choi, Y., Y. Wang, T. Zeng, R. V. Martin, T. P. Kurosu, and K. Chance (2005), Evidence of lightning NO<sub>x</sub> and convective transport of pollutants in satellite observations over North America, *Geophys. Res. Lett.*, **32**, L02805, doi:10.1029/2004GL021436.
- Crawford, J. H., and K. E. Pickering (2011), DISCOVER-AQ observations over the Baltimore-DC area during July 2011, Abstract A21J-01 presented at 2011 Fall Meeting, AGU, San Francisco, Calif., 5–9 Dec.
- D'Sa, E. J., and R. L. Miller (2003), Bio-optical properties in waters influenced by the Mississippi River during low flow conditions, *Remote Sens. Environ.*, **84**, 538–549.
- Davis, D. D., G. Grodzinsky, P. Kasibhatla, J. Crawford, G. Chen, S. Liu, A. Bandy, D. Thornton, H. Guan, and S. Sandholm (2001), Impact of ship emissions on marine boundary layer NO<sub>x</sub> and SO<sub>2</sub> distributions over the Pacific Basin, *Geophys. Res. Lett.*, **28**, 235–238.
- Doxaran, D., R. C. N. Cherukuru, and S. J. Lavender (2005), Use of reflectance band ratios to estimate suspended and dissolved matter concentrations in estuarine waters, *Int. J. Remote Sens.*, **26**(8), 1763–1769.
- Endresen, Ø., E. Sørgard, J. K. Sundet, S. B. Dalsøren, I. S. A. Isaksen, T. F. Berglen, and G. Gravir (2003), Emission from international sea transportation and environmental impact, *J. Geophys. Res.*, **108**(D17), 4560, doi:10.1029/2002JD002898.
- Fishman, J., et al. (2012), The United States' Next Generation of Atmospheric Composition and Coastal Ecosystem Measurements: NASA's Geostationary Coastal and Air Pollution Events (GEO APE) Mission, *Bull. Am. Meteorol. Soc.*, **93**, 1547–1566, doi:10.1175/BAMS-D-11-00201.1.
- Franke, K., A. Richter, H. Bovensmann, V. Eyring, P. Jöckel, P. Hoor, and J. P. Burrows (2009), Ship emitted NO<sub>2</sub> in the Indian Ocean: Comparison of model results with satellite data, *Atmos. Chem. Phys.*, **9**, 7289–7301.
- Gitelson, A. A., J. F. Schalles, and C. M. Hladik (2007), Remote chlorophyll-a retrieval in turbid, productive estuaries: Chesapeake Bay case study, *Remote Sens. Environ.*, **109**, 464–472, doi:10.1016/j.rse.2007.01.016.
- Goldberg, D. L., C. P. Loughner, M. Tzortziou, J. W. Stehr, K. E. Pickering, L. T. Marufu, and R. Dickerson (2014), Higher surface ozone concentrations over the Chesapeake Bay than over the adjacent land: Observations and models from the DISCOVER-AQ and CBODAQ campaigns, *Atmos. Environ.*, **84**, 9–19, doi:10.1016/j.atmosenv.2013.11.008.
- Gordon, H. R., and K. J. Voss (1999), *MODIS Normalized Water-Leaving Radiance, Algorithm Theoretical Basis Document (MOD 18), Version 4*, NASA Technic Document NAS5-31363, 93 pp., University of Miami, Coral Gables, Fla.
- Gordon, H. R., and M. Wang (1994), Retrieval of water-leaving radiance and aerosol optical thickness over the oceans with SeaWiFS: A preliminary algorithm, *Appl. Opt.*, **33**, 443–452.
- Gu, B., Y. Zhu, J. Chang, C. Peng, D. Liu, Y. Min, W. Luo, R. W. Howarth, and Y. Ge (2011), The role of technology and policy in mitigating regional nitrogen pollution, *Environ. Res. Lett.*, **6**, 014011.
- Guttikunda, S. K., Y. Tang, G. R. Charnichael, G. Kurata, L. Pan, D. G. Streets, J.-H. Woo, N. Thongboonchoo, and A. Fried (2005), Impacts of Asian megacity emissions on regional air quality during spring 2001, *J. Geophys. Res.*, **110**, D20301, doi:10.1029/2004JD004921.
- Harder, J. W., J. W. Brault, P. V. Johnston, and G. H. Mount (1997), Temperature dependent NO<sub>2</sub> cross sections at high spectral resolution, *J. Geophys. Res.*, **102**, 3861–3879.
- He, H., et al. (2014), An elevated reservoir of air pollutants over the Mid-Atlantic States during the 2011 DISCOVER-AQ campaign: Airborne measurements and numerical simulations, *Atmos. Environ.*, **85**, 18–30, doi:10.1016/j.atmosenv.2013.11.039.
- Herman, J. R., and M. Tzortziou (2011), Atmospheric correction for NO<sub>2</sub> absorption in coastal and estuarine environments and effects on ocean color retrievals, paper presented at 2nd GEO-CAPE Community Workshop, Boulder, Colo., 11–13 May.
- Herman, J. R., A. Cede, E. Spinei, G. Mount, M. Tzortziou, and N. Abuhassan (2009), NO<sub>2</sub> column amounts from ground-based Pandora and MFDOAS spectrometers using the Direct-Sun DOAS technique: Intercomparisons and application to OMI validation, *J. Geophys. Res.*, **114**, D13307, doi:10.1029/2009JD011848.
- Holben, B. N., et al. (1998), AERONET—A federated instrument network and data archive for aerosol characterization, *Remote Sens. Environ.*, **66**, 1–16.
- IOCCG (2010), Atmospheric correction for remotely-sensed ocean-colour products, in *Reports of the International Ocean-Colour Coordinating Group*, edited by M. Wang, 78 pp., Dartmouth, Canada.
- IOCCG (2012), Ocean-colour observations from a geostationary orbit, in *Reports of the International Ocean-Colour Coordinating Group*, edited by D. Antoine, 102 pp., Dartmouth, Canada.
- Johannessen, S. C., W. L. Miller, and J. J. Cullen (2003), Calculation of UV attenuation and colored dissolved organic matter absorption spectra from measurements of ocean color, *J. Geophys. Res.*, **108**(C9), 3301, doi:10.1029/2000JC000514.
- Kahru, M., and B. G. Mitchell (2001), Seasonal and nonseasonal variability of satellite-derived chlorophyll and colored dissolved organic matter concentration in the California current, *J. Geophys. Res.*, **106**, 2517–2529.
- Kallos, G., P. Kassomenos, and R. A. Pielke (1993), Synoptic and mesoscale weather conditions during air pollution episodes in Athens, Greece, *Boundary Layer Meteorol.*, **62**, 163–184.
- Kanakidou, M., et al. (2011), Megacities as hot spots of air pollution in the East Mediterranean, *Atmos. Environ.*, **45**(6), 1223–1235.
- Krotkov, N. A., and OMI NO<sub>2</sub> Algorithm Team (2012), OMNO2 README file, Document Version 6.2, NASA Goddard Space Flight Cent., Greenbelt, Md. [Available at [http://disc.sci.gsfc.nasa.gov/Aura/data-holdings/OMI/documents/v003/OMNO2\\_readme\\_v003.pdf](http://disc.sci.gsfc.nasa.gov/Aura/data-holdings/OMI/documents/v003/OMNO2_readme_v003.pdf), last accessed 31 Jul. 2012.]
- Krotkov, N. A., P. K. Bhartia, J. R. Herman, and J. Slusser (2005), Measuring aerosol UV absorption optical thickness by combining use of shadowband and almucantar techniques, in *Ultraviolet Ground- and Space-Based Measurements, Models, and Effects IV*, edited by J. R. Slusser, J. R. Herman, W. Gao, and G. Bernhard, pp. 17–27, Proc. SPIE 5545, Bellingham, Wash., doi:10.1117/12.559557.
- Le, C., and C. Hu (2013), A hybrid approach to estimate chromophoric dissolved organic matter in turbid estuaries from satellite measurements: A case study for Tampa Bay, *Opt. Express*, **21**(16), 18,849–18,871, doi:10.1364/OE.21.018849.
- Le, C., C. Hu, J. Cannizzaro, D. English, F. Muller-Karger, and Z. Lee (2013), Evaluation of chlorophyll-a remote sensing algorithm for an optically complex estuary, *Remote Sens. Environ.*, **129**, 75–89.
- Lee, D. S., I. Kohler, E. Grobler, F. Rohrer, R. Sausen, L. Gallardo-Klenner, J. G. J. Olivier, F. J. Dentener, and A. F. Bouwman (1997), Estimations of global NO<sub>x</sub> emissions and their uncertainties, *Atmos. Environ.*, **31**, 1735–1749.
- Levelt, P. F., G. H. J. van den Oord, M. R. Dobber, A. Mäkkij, H. Visser, J. de Vries, P. Stammes, J. O. V. Lundell, and H. Saari (2006), The ozone monitoring instrument, *IEEE Trans. Geosci. Remote Sens.*, **44**(5), 1093–1101.
- Loughner, C. P., D. J. Allen, K. E. Pickering, R. R. Dickerson, D.-L. Zhang, and Y.-X. Shou (2011), Impact of the Chesapeake Bay breeze and fair-weather cumulus clouds on pollutant transport and transformation, *Atmos. Environ.*, **45**, 4060–4072.
- Loughner, C. P., M. Tzortziou, M. Duffy, B. Duncan, J. Hains, K. E. Pickering, Y. Yoshida, and M. Follette-Cook (2013), Impact of historical air pollution emissions reductions on nitrogen deposition, Abstract B41H-02 presented at 2013 AGU Fall Meeting, San Francisco, Calif., 9–13 Dec.

- Loughner, C. P., et al. (2014), Impact of bay breeze circulations on surface air quality and boundary layer export, *J. Appl. Meteorol. Climatol.*, doi:10.1175/JAMC-D-13-0323.1, in press.
- Martini, L. A., et al. (2006), Sources of reactive nitrogen affecting ecosystems in Latin America and the Caribbean: current trends and future perspectives, *Biogeochemistry*, 79, 3–24, doi:10.1007/s10533-006-9000-3.
- Mannino, A., M. E. Russ, and S. B. Hooker (2008), Algorithm development for satellite-derived distributions of DOC and CDOM in the U.S. Middle Atlantic Bight, *J. Geophys. Res.*, 113, C07051, doi:10.1029/2007JC004493.
- Mobley, C. D. (1988), A numerical model for the computation of radiance distribution in natural waters with wind-roughened surfaces, Part II: User's guide and code listing, *NOAA Tech. Memo ERL PMEL-81 (NTIS PB88e246871)*, Pacific Mar. Environ. Lab., Seattle, Wash.
- Mobley, C. D. (1994), *Light and Water, Radiative Transfer in Natural Waters*, Academic, San Diego, Calif.
- O'Reilly, J. E., et al. (2000), Ocean color chlorophyll a algorithms for SeaWiFS, OC2, and OC4: Version 4. SeaWiFS postlaunch calibration and validation analyses, Part 3, *NASA Tech. Memo. 2000-206892*, vol. 11, NASA Goddard Space Flight Cent., Greenbelt, Md.
- Osburn, C. L., H. E. Zagarese, W. Cravero, D. P. Morris, and B. R. Hargreaves (2001), Calculation of spectral weighting functions for the solar photobleaching of chromophoric dissolved organic matter in temperate lakes, *Limnol. Oceanogr.*, 46, 1455–1467.
- PACE Science Definition Team (SDT) (2012), A report of the pre-aerosol, clouds, and ocean ecosystem (PACE) mission (Chair: C. Del Castillo), 271 pp., Johns Hopkins Univ. Appl. Phys. Lab., Laurel, Md. [Available at [http://dsm.gsfc.nasa.gov/pace\\_documentation/PACE\\_SDT\\_Report\\_final.pdf](http://dsm.gsfc.nasa.gov/pace_documentation/PACE_SDT_Report_final.pdf)].
- Palmer, P. I., D. J. Jacob, K. Chance, R. V. Martin, R. J. D. Spurr, T. P. Kurosu, I. Bey, R. Yantosca, and A. Fiore (2001), Air mass factor formulation for spectroscopic measurements from satellites: Application to formaldehyde retrievals from the Global Ozone Monitoring Experiment, *J. Geophys. Res.*, 106, 14,539–14,550.
- Pandey, S. K., K. H. Kim, S. Y. Chung, S. J. Cho, M. Y. Kim, and Z. H. Shon (2008), Long-term study of NO<sub>x</sub> behavior at urban roadside and background locations in Seoul, Korea, *Atmos. Environ.*, 42(4), 607–622.
- Pineda Rojas, A. L., and L. E. Venegas (2009), Atmospheric deposition of nitrogen emitted in the Metropolitan Area of Buenos Aires to coastal waters of de la Plata River, *Atmos. Environ.*, 43, 1339–1348.
- Platt, U. (1994), Differential optical absorption spectroscopy (DOAS), in *Air Monitoring by Spectroscopic Techniques*, *Chem. Anal. Ser.*, vol. 127, edited by M. W. Sigrist, pp. 27–76, John Wiley, N. Y.
- Reed, A., A. M. Thompson, D. E. Kollonige, D. K. Martins, M. Tzortziou, J. R. Herman, T. A. Berkoff, N. K. Abuhassan, and A. Cede (2013), Effects of local meteorology and aerosols on ozone and nitrogen dioxide retrievals from OMI and Pandora spectrometers in Maryland, USA during DISCOVER-AQ 2011, *J. Atmos. Chem.*, doi:10.1007/s10874-013-9254-9.
- Richter, A., V. Eyring, J. P. Burrows, H. Bovensmann, A. Lauer, B. Sierk, and P. J. Crutzen (2004), Satellite measurements of NO<sub>2</sub> from international shipping emissions, *Geophys. Res. Lett.*, 31, L23110, doi:10.1029/2004GL020822.
- Richter, A., J. P. Burrows, H. Nüßlig, C. Granier, and U. Niemeier (2005), Increase in tropospheric nitrogen dioxide over China observed from space (and supplementary discussion on: Error estimates for changes in tropospheric NO<sub>2</sub> columns as derived from satellite measurements), *Nature*, 437, 129–132, doi:10.1038/nature04092.
- Robinson, W., Z. Ahmad, and C. McClain (2007), A temporally consistent NO<sub>2</sub> data record for ocean color work, paper presented at Tropospheric NO<sub>2</sub> Measured by Satellites Workshop, KNMI, DeBilt, Netherlands, 10–12 Sep.
- Ruddick, K. G., F. Ovidio, and M. Rijkeboer (2000), Atmospheric correction of SeaWiFS imagery for turbid coastal and inland waters, *Appl. Opt.*, 39, 897–912.
- Ruddick, K. G., H. J. Gons, M. Rijkeboer, and G. Tilstone (2001), Optical remote sensing of chlorophyll a in case 2 waters by use of an adaptive two-band algorithm with optimal error properties, *Appl. Opt.*, 40(21), 3575–3585.
- Siegel, D. A., M. Wang, S. Maritorena, and W. Robinson (2000), Atmospheric correction of satellite ocean color imagery: The black pixel assumption, *Appl. Opt.*, 39, 3582–3591.
- Skamarock, W. C., J. B. Klemp, J. Dudhia, D. O. Gill, D. M. Barker, W. Wang, and J. G. Powers (2008), A description of the advanced research WRF Version 3, *NCAR Tech. Note TN-468+STR*, 113 pp., Natl. Cent. for Atmos. Res., Boulder, Colo.
- Stumpf, R. P., R. A. Arnone, R. W. Gould, P. M. Martinovich, and V. Ransibrahmanakul (2003), A partially coupled ocean-atmosphere model for retrieval of water-leaving radiance from SeaWiFS in coastal waters, *NASA Tech. Memo. 206892, SeaWiFS Postlaunch Tech. Rep. Ser.*, edited by S. B. Hooker and E. R. Firestone, vol. 22, pp. 51–59, NASA Goddard Space Flight Cent., Greenbelt, Md.
- Tehrani, N. C., E. J. D'Sa, C. L. Osburn, T. S. Bianchi, and B. A. Schaeffer (2013), Chromophoric dissolved organic matter and dissolved organic carbon from Sea-Viewing Wide Field-of-View Sensor (SeaWiFS), moderate resolution imaging spectroradiometer (MODIS) and MERIS sensors: Case study for the Northern Gulf of Mexico, *Remote Sens.*, 5(3), 1439–1464.
- Tie, X., F. Geng, L. Peng, W. Gao, and C. Zhao (2009), Measurement and modeling of O<sub>3</sub> variability in Shanghai, China: Application of the WRF-Chem model, *Atmos. Environ.*, 43, 4289–4302.
- Tzortziou, M., J. Herman, C. Gallegos, P. Neale, A. Subramaniam, L. Harding, and Z. Ahmad (2006), Bio-optics of the Chesapeake Bay from measurements and radiative transfer closure, *Estuarine Coastal Shelf Sci.*, 68(2), 348–362, doi:10.1016/j.ecss.2006.02.016.
- Tzortziou, M., A. Subramaniam, J. Herman, C. Gallegos, P. Neale, and L. Harding (2007), Remote sensing reflectance and inherent optical properties in the Mid Chesapeake Bay, *Estuarine Coastal Shelf Sci.*, 72(1), 16–32, doi:10.1016/j.ecss.2006.09.018.
- Tzortziou, M., J. R. Herman, A. Cede, and N. Abuhassan (2012), High precision, absolute total column ozone measurements from the Pandora spectrometer system: Comparisons with data from a Brewer double monochromator and Aura OMI, *J. Geophys. Res.*, 117, D16303, doi:10.1029/2012JD017814.
- Tzortziou, M., J. R. Herman, C. P. Loughner, A. Cede, N. Abuhassan, and S. Naik (2013), Spatial and temporal variability of ozone and nitrogen dioxide over a major urban estuarine ecosystem, *J. Atmos. Chem.*, doi:10.1007/s10874-013-9255-8.
- Vandaele, A. C., C. Hermans, P. C. Simon, M. Carleer, R. Colin, S. Fally, M. F. Mérienne, A. Jenouvrier, and B. Coquart (1998), Measurements of the NO<sub>2</sub> absorption cross-section from 42 000 cm<sup>-1</sup> to 10 000 cm<sup>-1</sup> (238–1000 nm) at 220 K and 294 K, *J. Quant. Spectrosc. Radiat. Transfer*, 59(3–5), 171–184.
- von Glasow, R., et al. (2013), Megacities and large urban agglomerations in the coastal zone: Interactions between atmosphere, land, and marine ecosystems, *Ambio*, 42(1), 13–28, doi:10.1007/s13280-012-0343-9.
- Wang, M., W. Shi, and L. Jiang (2012), Atmospheric correction using near-infrared bands for satellite ocean color data processing in the turbid western Pacific region, *Opt Express*, 20(2), 741–753, doi:10.1364/OE.20.000741.
- Wenig, M., N. Spichtinger, A. Stohl, G. Held, S. Beirle, T. Wagner, B. Jahne, and U. Platt (2003), Intercontinental transport of nitrogen oxide pollution plumes, *Atmos. Chem. Phys.*, 3, 387–393.